

Surface Wrinkling: A Versatile Platform for Measuring Thin-Film Properties

Jun Young Chung, Adam J. Nolte, and Christopher M. Stafford*

Surface instabilities in soft matter have been the subject of increasingly innovative research aimed at better understanding the physics of their formation and their utility in patterning, organizing, and measuring materials properties on the micro and nanoscale. The focus of this Review is on a type of instability pattern known as surface wrinkling, covering the general concepts of this phenomenon and several recent applications involving the measurement of thin-film properties. The ability of surface wrinkling to yield new insights into particularly challenging materials systems such as ultrathin films, polymer brushes, polyelectrolyte multilayer assemblies, ultrasoft materials, and nanoscale structured materials is highlighted. A perspective on the future directions of this maturing field, including the prospects for advanced thin-film metrology methods, facile surface patterning, and the control of topology-sensitive phenomena, such as wetting and adhesion, is also presented.

1. Introduction

A variety of complex, self-organized patterns are evident in nature, from microscopic phenomena, such as molecular crystallinity and composite layering in seashell nacre, to visible- and even astronomical-scale structures, such as the ripples in sand dunes and the organization of stars and larger clusters of galaxies throughout space. The ubiquity and diversity of self-organization phenomena in nature has spurred new research efforts, with scientists attempting to design artificial systems that will spontaneously develop similarly rich and complex patterns.

In particular, instability phenomena in thin films have received increasing attention due to the ease of using self-organization in such systems to generate well-defined and complex topological features.^[1–3] Spontaneous formation of highly ordered surface wrinkles represents one class of instability-driven self-organization,^[4–18] and examples are readily apparent in natural systems, such as aging human skin and dried fruit.^[8,16] Similar phenomena can be easily obtained in

engineered systems by compressing a thin, stiff film attached to a compliant substrate. Such systems give rise to wrinkling patterns that can display rich surface morphologies and multiple-scale ordering; the applied stress state can be controlled by methods such as mechanical compression,^[10–12] thermal expansion^[9,17] and swelling or shrinkage.^[14,15,18] In all cases, planar compressive forces cause wrinkling of the film at a characteristic wavelength that minimizes the total energy due to bending in the film and deformation of the substrate. The wrinkling wavelength is proportional to the cube root of the ratio of the elastic moduli of the film and substrate, multiplied by the film thickness (see Section 2 below).^[19] Since the early work of Whitesides and coworkers,^[4–6] significant progress in theoretical and

experimental studies has led to greater physical understanding of surface instability phenomena, spurring research interest in engineering topologically self-organizing systems across many length scales.

The metrological application of instability patterns in films has been a more recent development, whereby the characteristic length scale of an instability pattern is used to characterize material properties; in this case, understanding the self-organization process is a key step in translating geometric measurements of the wavelength and amplitude into material property values. A number of innovative techniques have been developed in this vein, a partial list of which includes measurements of thickness using fingering instabilities in thin elastic films,^[20] Poisson's ratio through wrinkling of stretched elastic sheets,^[21] residual stress through dewetting of thin polymer films,^[22] modulus through contact instabilities between dissimilar elastic films,^[23] and thickness and modulus through capillary wrinkling of floating thin films.^[24] Cerda and coworkers have even recently demonstrated that the geometric shape of the apex of a torn piece of film (such as wallpaper)^[25] and the geometric patterns seen at biological interfaces^[26] can be used to determine material properties.

Among this wide variety of instability-based characterization techniques, surface wrinkling has occupied a place of particular importance due to its ease and applicability to a wide variety of systems. Pioneering work in the early 2000s in the Polymers Division of the National Institute of Standards and Technology (NIST) showed that mechanically induced wrinkling instabilities allow one to directly measure the elastic modulus

Dr. J. Y. Chung, Dr. A. J. Nolte,^[+] Dr. C. M. Stafford
Polymers Division
National Institute of Standards and Technology
100 Bureau Drive, Gaithersburg, MD 20899, USA
E-mail: chris.stafford@nist.gov

[+] Present Address: Department of Chemical Engineering
Rose-Hulman Institute of Technology, Terre Haute, IN 47803, USA

DOI: 10.1002/adma.201001759

of polymer thin films and coatings.^[10] A key advantage of this technique is that the elastic modulus of a nanoscale film can be calculated after measuring the (typically) microscale (and thus easy to observe) wrinkling wavelength of the film. Thus, this technique avoids many difficulties inherent to methods such as nanoindentation, where uncertainties associated with indentation depth and the proximity of the substrate can lead to considerable error in the measured elastic modulus of ultrathin polymer films.^[27–29] In addition to accommodating the challenges of small specimens (even for films as thin as a few nanometers)^[30], surface wrinkling allows for in situ evaluation and high-throughput measurement capabilities,^[31] and the typical wrinkle wavelength is generally small enough to accurately measure heterogeneities (differences in local elastic modulus) down to the micrometer scale.^[32] Furthermore, this method is simple and inexpensive to implement, thereby lowering the barrier for widespread application of the technique. As evidence of this latter point, in just the past few years the use of surface wrinkling outside of NIST has grown significantly, and its applicability has already been demonstrated on a variety of materials systems, including ultrathin polymer films,^[30,33] polyelectrolyte multilayer assemblies,^[32,34,35] ultrasoft materials,^[36] thin metal films,^[4,37] polymer brushes,^[38,39] carbon nanotubes,^[40] photore-sist materials,^[41] hybrid nanomembranes,^[32,42,43] hybrid interpenetrated network nanofilms,^[44] polymer nanocomposites,^[45] porous materials,^[10,46] and organic electronic materials.^[47]

In this Review, we offer our perspective on the development and use of surface wrinkling as a tool for characterizing materials and creating surfaces with functional patterned topology. Because of the rapid growth in this area, a comprehensive review remains beyond the scope of this paper; wrinkling is being increasingly employed in a variety of novel applications, with examples including microfluidics, tunable phase gratings, and stretchable electronics. Excellent discussions of these and other topics can be found elsewhere.^[13,48,49] Here we will emphasize the basic physics explaining wrinkling behavior, and focus on wrinkling-based measurement strategies that have been recently developed to obtain otherwise difficult-to-measure properties of thin-film materials. Finally, we will conclude with an overview of current applications of surface wrinkling for systematically studying topography-driven phenomena, and offer perspectives for future work in this rich and exciting field.

2. Wrinkling Mechanics and Measurements

The mathematical study of instability phenomena dates back at least to the work of Euler in the 18th century. His detailed analysis of buckling in struts and columns predicted the onset of an elastic instability when the applied axial compressive load on a column exceeds some critical value, at which point the column becomes unstable and undergoes a lateral displacement away from the centerline axis.^[50] This elastic instability is known as buckling, and the critical load for buckling is generally less than the ultimate strength of the column material. The formula derived by Euler established that the critical load for buckling is a function of the bending rigidity of the column and is inversely proportional to the column length.



Jun Young Chung received his Ph.D. in chemical engineering in 2006 from Lehigh University, under the supervision of Prof. Manoj K. Chaudhury. He is currently a research associate in the Polymers Division at the National Institute of Standards and Technology. His current research interests include surface wrinkling

metrology, self-organized patterning, and bioinspired materials design, as well as adhesion, friction and fracture at soft interfaces.



Adam J. Nolte is an assistant professor in the Department of Chemical Engineering at the Rose-Hulman Institute of Technology. He formerly worked as a materials research engineer in the Polymers Division at the National Institute of Standards and Technology. He received his Ph.D. in materials science and engineering from

the Massachusetts Institute of Technology in 2007. His current research interests include polymer thin films, layer-by-layer assembly, interfacial adhesion, and the optical and mechanical properties of nanostructured, layered materials.



Christopher M. Stafford is a staff scientist and project leader in the Polymers Division at the National Institute of Standards and Technology. He received his Ph.D. in polymer science and engineering from the University of Massachusetts, Amherst in 2001. His current research is focused on measuring the effects of complex

interfaces on the structure, properties, and dynamics of soft materials, as well as measuring the effects of environmental factors on the performance and degradation of sustainable materials and coatings.

In the mid-20th century, a similar analysis was applied to laminates in the form of sandwich panels, the simplest of which is comprised of two relatively thin, stiff sheets of material bonded to either surface of a thick, compliant material.^[19,51] Upon compressive loading, a buckling-type instability can

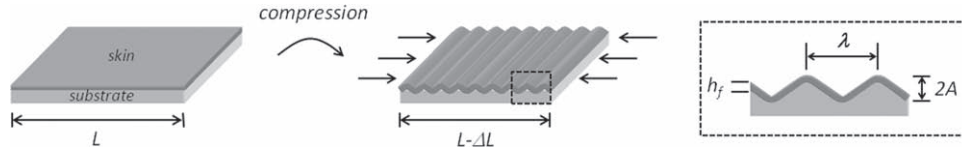


Figure 1. Schematic of surface wrinkling of a laminate structure comprised of a stiff skin adhered to a soft substrate. The laminate undergoes wrinkling upon compressive strain from an initial length (L) to a final length ($L-\Delta L$).

occur on the surface of the laminate, where the surface begins to wrinkle with a defined wavelength and amplitude. This phenomenon is illustrated in **Figure 1**. The wavelength of the wrinkling instability (λ) in such a laminate is linearly dependent on the thickness (h) of the skin ($\lambda \sim h$). Additionally, the amplitude of the wrinkles (A) increases nonlinearly with strain (ϵ) as $A \sim \epsilon^{1/2}$. In order to more clearly illustrate the fundamental physical foundation and common framework for the research and applications discussed in this Review, we will briefly derive the underlying mechanics equations for the wrinkling wavelength, critical strain, and amplitude.

Surface wrinkling can be described using either a force balance^[52–54] or an energy balance.^[8,21,55] Here, the force balance approach will be described in some detail. While originally derived for bending of a long, thin beam on a semi-infinite substrate (plane-stress condition), most examples in the literature involve the use of films (plates) on semi-infinite substrates (plane-strain condition). Therefore, we will consider the latter case here. The classical equation for bending of a stiff film on a more compliant, elastic substrate is:

$$\bar{E}_f I \frac{d^4 z}{dx^4} + F \frac{d^2 z}{dx^2} + kz = 0, \quad (1)$$

where $\bar{E} = E/(1-\nu^2)$ is the plane-strain modulus, E is the Young's modulus, ν is the Poisson's ratio, $I = wh^3/12$ is the moment of inertia (where w is the width of the film and h is its thickness), F is the uniaxially applied force or load, and k is the Winkler's modulus of an elastic half-space ($k = \bar{E}_s w \pi / \lambda$).^[56] The subscripts, f and s , denote the film and substrate, respectively. The z -axis is defined to be normal to the surface and the x -axis parallel to the direction of F . In Equation 1, the first and third terms belong to the classical Euler–Bernoulli beam-bending equation that equates bending forces in the film with the normal force distribution due to deformation of the substrate above and below its neutral position. The second term incorporates the effects of the force, F , on the film. In contrast to buckling of a column, wrinkling of a film on an elastic foundation involves a balance of force between film bending (first term in Equation 1), which acts to suppress short wavelengths, and substrate deformation (third term in Equation 1), which acts to suppress large wavelengths. We assume that the instability can be described by a sinusoidal vertical deflection of the film:

$$z(x) = A \sin \frac{2\pi x}{\lambda}. \quad (2)$$

Substituting Equation 2 into Equation 1 yields:

$$16 \bar{E}_f I \left(\frac{\pi}{\lambda}\right)^4 z - 4F \left(\frac{\pi}{\lambda}\right)^2 z + \bar{E}_s w \left(\frac{\pi}{\lambda}\right) z = 0. \quad (3)$$

Solving for the applied force in the system yields:

$$F = 4 \bar{E}_f I \left(\frac{\pi}{\lambda}\right)^2 + \frac{\bar{E}_s w}{4} \left(\frac{\pi}{\lambda}\right)^{-1}. \quad (4)$$

Differentiating Equation 4 with respect to wavelength and setting this equal to zero (i.e., $\partial F / \partial \lambda = 0$) yields a wavelength that minimizes F :

$$\lambda = 2\pi h \left(\frac{\bar{E}_f}{3\bar{E}_s}\right)^{\frac{1}{3}}. \quad (5)$$

Equation 5 is the basis of the surface wrinkling metrology, as will be described later.

Another key parameter is the amount of stress or strain needed to induce wrinkling in the system. The critical stress (σ_c) can be determined from Equation 4 and Equation 5 by dividing the applied force at the critical point (F_c) by the cross-sectional area of the film:

$$\sigma_c = \frac{F_c}{hw} = \left(\frac{9}{64} \bar{E}_f \bar{E}_s^2\right)^{\frac{1}{3}}. \quad (6)$$

Thus, the critical strain (ϵ_c) is

$$\epsilon_c = \frac{\sigma_c}{\bar{E}_f} = \frac{1}{4} \left(\frac{3\bar{E}_s}{\bar{E}_f}\right)^{\frac{2}{3}}. \quad (7)$$

Note that ϵ_c only depends on the modulus ratio of the substrate and film and the thickness of the film does not affect ϵ_c .

Once the applied strain exceeds the critical strain and a wrinkling wavelength is established, further strain is accommodated in large part by increasing the amplitude (A) of the wrinkling instability, while λ remains approximately constant (by Equation 5, λ is independent of ϵ). In reality, it has been shown that there is a decrease in the wrinkling wavelength with increasing strain,^[57,58] although for strains <10% this decrease can generally be neglected.^[59]

With the assumption that λ is independent of ϵ , an expression for the wrinkling amplitude can be derived by assuming that the release of tensile strain in the system, upon onset of the instability, is equal to the overstrain ($\epsilon - \epsilon_c$), which is the difference between the applied strain and the strain needed to induce the instability. This relationship can be expressed as:

$$\epsilon - \epsilon_c = \frac{1}{\lambda} \int_0^\lambda \sqrt{1 + \left(\frac{dz}{dx}\right)^2} dx - 1 \quad (8)$$

where the integral in Equation 8 represents the contour length of the wrinkled film over one period of the instability. By substituting Equation 2 into Equation 8 and assuming that

$$\sqrt{1 + \left(\frac{dz}{dx}\right)^2} \approx 1 + \frac{1}{2} \left(\frac{dz}{dx}\right)^2 \quad (9)$$

since $A \ll \lambda$ and hence dz/dx is small, one obtains

$$\varepsilon - \varepsilon_c = \frac{\pi^2 A^2}{\lambda^2}. \quad (10)$$

Finally, combining Equation 5, Equation 7, and Equation 10 yields an expression relating wrinkle amplitude to strain:

$$A = h \sqrt{\frac{\varepsilon - \varepsilon_c}{\varepsilon_c}}. \quad (11)$$

The above three parameters (ε_c , λ , A) capture the central aspects of surface wrinkling: the strain at which the wrinkling instability occurs, the wavelength of the instability, and the amplitude growth as a function of strain.

Experimentally, there are several measurement tools that can be used to ascertain one or more of these three parameters simultaneously.^[31,60] The simplest and most widely available method is optical microscopy (OM) operated in reflectance mode. **Figure 2a** shows representative OM images of wrinkled surfaces resulting from uniaxial (top) and isotropic (bottom) compression. λ can be calculated either in real space using the distance averaged over multiple waves or in reciprocal space using a fast Fourier transform (FFT). FFT is preferred since it quickly provides the average wavelength across the entire image, rather than point-by-point measurements in real space. Unfortunately, traditional OM does not easily provide a measure of the wrinkling amplitude. Higher amplitudes simply

yield higher contrast between the peaks and valleys of the wrinkled surface. In addition, it is difficult to observe ε_c accurately using OM due to the poor contrast of low amplitude wrinkles. It might be possible to use OM with z-stack image acquisition via high-resolution piezo-electric drives to measure A (and thus ε_c), while optical profilometry might also be able to detect all three parameters, although we are not aware of any reported attempts to pursue such techniques. We have instead relied on direct surface imaging techniques such as atomic force microscopy (AFM) or stylus profilometry to measure ε_c , λ , and A simultaneously.^[30,59]

Figure 2b shows AFM images of wrinkled surfaces, where both λ and A can be determined from image analyses such as power spectral density, FFT, and/or roughness functions. The accuracy of determining λ is a convolution of the particular function employed and the size of the image. For example, a section analysis is best used on images containing a small number of wavelengths in order to maximize the resolution of each pixel. Conversely, FFT minimizes measurement error for images that are large in relation to the wavelength spacing. If outfitted with a strain stage, AFM can also detect the onset of wrinkling by providing a measure of the amplitude as a function of strain.^[59] At low strains, the sample remains flat and featureless, but once ε_c is reached the surface becomes corrugated due to the wrinkling instability. As the strain is increased, the amplitude increases according to Equation 11. This is shown in **Figure 3**; in this example, the critical strain was found to be $\approx 1\%$ for polystyrene (PS) on poly(dimethylsiloxane) (PDMS). One of the disadvantages to using surface imaging techniques such as AFM to determine ε_c , λ , and A is the relatively low throughput of these techniques; for example, the data in **Figure 3** took ≈ 1 day to collect. However, the resolution and sensitivity of AFM is unparalleled, and this may be necessary for certain studies.

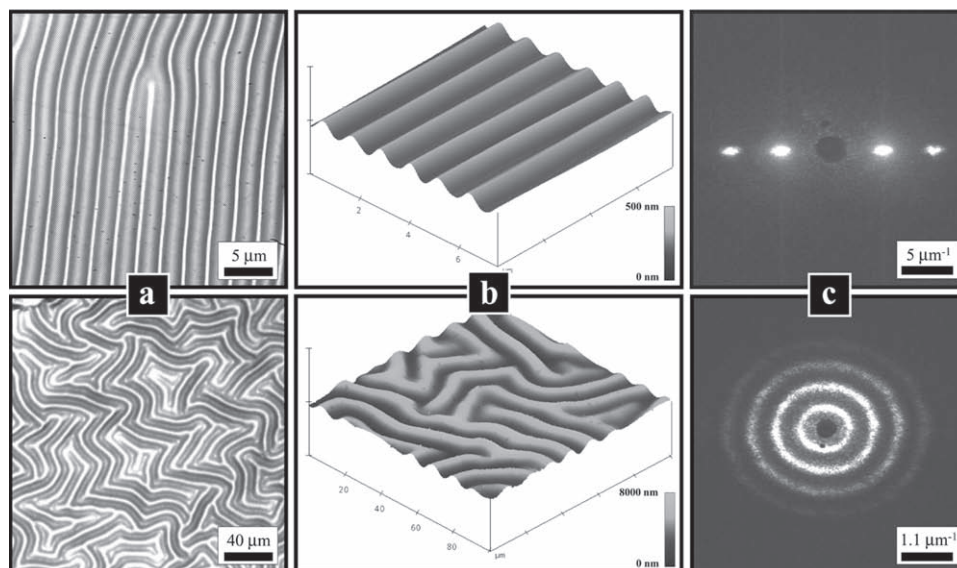


Figure 2. Examples of different methods for measuring the wrinkling wavelength for both uniaxial compression (top) and isotropic compression (bottom): a) optical microscopy, b) atomic force microscopy, and c) small-angle light scattering. The advantages and disadvantages of each technique are discussed in the text. Reproduced with permission.^[60] Copyright 2006, Elsevier.

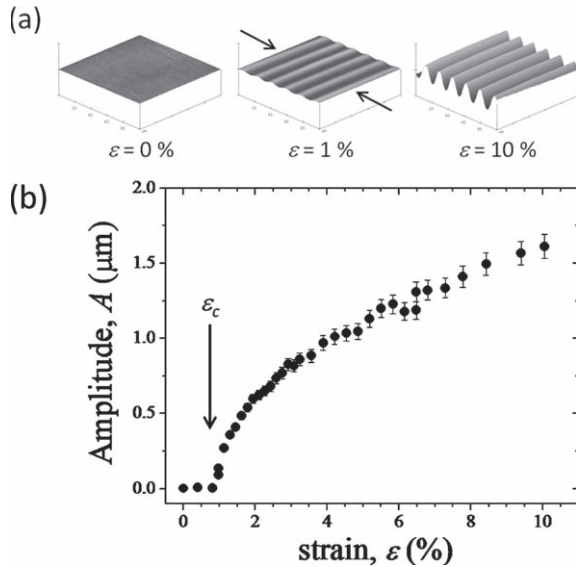


Figure 3. Demonstration of AFM to detect both the critical strain (ϵ_c) for wrinkling as well as the amplitude (A) of the wrinkle pattern. a) AFM images showing the transition from a flat film to a wrinkled surface as compressive strain is increased. Note that going from 1% to 10% strain, the number of wrinkles in the AFM image remains constant while the amplitude increases an order of magnitude. b) Amplitude as a function of applied strain, showing both the critical strain and the amplitude increasing non-linearly with strain. The error bars represent one standard deviation of the data, which is taken as the experimental uncertainty of the measurement. Reproduced with permission.^[59] Copyright 2004, AIP.

We have also shown that small angle light scattering (SALS) is an efficient means for quickly and accurately obtaining λ and ϵ_c (see Figure 2c and Figure 4).^[10,31,60–62] In SALS, a laser beam is transmitted through the sample and projected onto a screen.

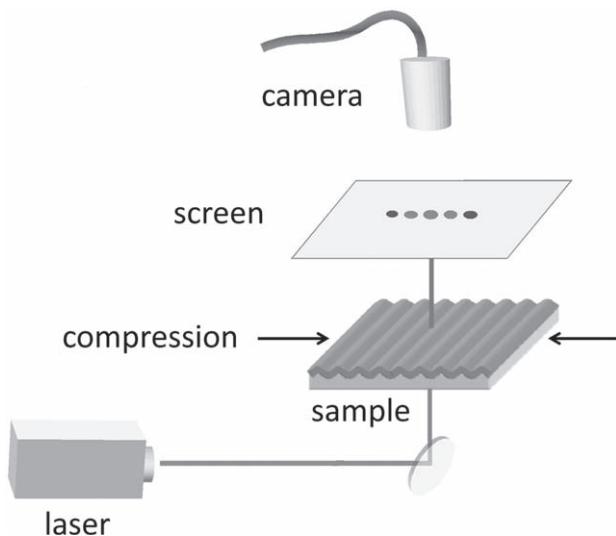


Figure 4. Schematic of the SALS apparatus for rapidly measuring λ and ϵ_c . This particular geometry is applicable to transparent samples; surface scattering via reflection is applicable to samples that are opaque or reflective. Reproduced with permission.^[10] Copyright 2004, Nature Publishing Group.

If the sample contains periodic structure, diffraction of the laser will occur with a dominant scattering wave vector, q_0 , which is related to the wavelength of the pattern as:

$$q_0 = \frac{2\pi}{\lambda}. \quad (12)$$

Below ϵ_c , the film remains flat and only the primary (non-diffracted) beam is detected. Above ϵ_c , diffraction occurs due to the periodic undulation (wrinkling) of the surface. As the strain is increased further, the amplitude, and hence scattering efficiency, of the wrinkles grows, leading to an increase in the intensity of the diffracted beam. The intensity of the diffracted beam is roughly proportional to the square of the wrinkling amplitude ($I \sim A^2$). For determining the value of ϵ_c , it is not necessary to have an absolute measure of amplitude; rather, a relative change in scattering intensity of the first-order diffraction spot is sufficient. It has been shown that first-order diffraction intensity can be approximated by a linear function at low strains.^[59,61] Thus, ϵ_c can be determined by extrapolating the scattered intensity to zero via linear regression. This progression is shown in Figure 5, where the critical strain was determined to be $\epsilon_c \approx 1\%$ for PS on PDMS. At the same time, λ can be measured from the position of the first-order diffraction peak (also shown in Figure 5). This particular approach is applicable only if the sample is optically transparent; if the sample is opaque, a similar geometry can be employed that makes use of scattering via surface reflection.^[62]

Having provided a description of the key parameters involved in surface wrinkling and a summary of how to experimentally measure them, the following section will focus on how such information may be integrated into metrological approaches for studying the material properties of thin film systems.

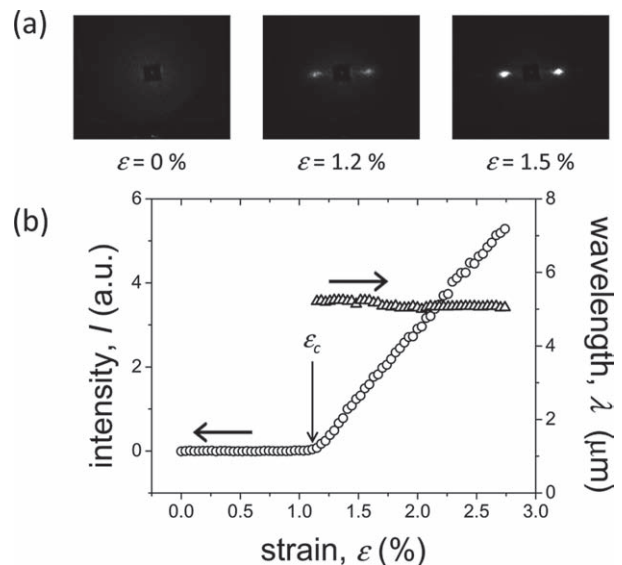


Figure 5. Demonstration of SALS to detect both the critical strain (ϵ_c) for wrinkling as well as the wavelength (λ) of the wrinkle pattern. a) Diffraction patterns illustrating the transition from a flat film to a wrinkled surface as compressive strain is increased. b) Scattering intensity, I , (circles) and λ (triangles) as calculated from the first-order diffraction peak as a function of applied strain. Reproduced with permission.^[61] Copyright 2009, ACS.

3. Modulus Measurements Via Surface Wrinkling

3.1. High-Throughput Measurement Strategies

From the above description of the mechanics governing the wrinkling of thin films on compliant substrates, a clear picture has begun to emerge on how to utilize the wrinkling instability phenomenon as a powerful metrology tool. The first published experiments to combine film thickness, wrinkling wavelength, and substrate modulus in a predictive fashion to determine the Young's modulus of thin films were performed at NIST on thin films of PS that were created by flow-coating.^[10,31] Thin films of PS with gradients in film thickness were prepared by using a flat blade to draw a toluene solution of PS across a Si surface with an accelerating speed.^[63] The gradient thickness samples were then transferred to PDMS substrates, and subjected to uniaxial compressive forces that wrinkled the film with a wavelength linearly proportional to the local film thickness, as shown in **Figure 6**. The linear relationship between film thickness and wrinkling wavelength, per Equation 5, indicates that the measured Young's modulus of the PS film is constant over this range of film thicknesses, and should be given by:

$$\bar{E}_f = 3 \bar{E}_s \left(\frac{\lambda}{2\pi h} \right)^3 \quad (13)$$

In fact, the PS modulus calculated using Equation 13 deviated little from its average value of 3.4 GPa \pm 0.1 GPa at all spots on the gradient, as shown in **Figure 6b**; this value is in excellent agreement with the measured bulk modulus of PS.^[10]

These preliminary experiments highlighted a number of important aspects concerning the importance of thin-film surface wrinkling as a new metrology technique. Most obvious was the relative ease with which the Young's modulus of a very thin film of soft material could be obtained. Such measurements had previously been extremely difficult to perform accurately. The advantage of surface wrinkling lies in the ability to use the straightforward theory of linear-elastic mechanics to relate the film modulus to otherwise easy-to-measure parameters; indeed, at NIST we have measured the wrinkling wavelength using a wide range of techniques including both mechanical (AFM and profilometry) and optical (laser light scattering and optical microscopy) approaches, as described in Section 2, while the thickness of the film can be likewise flexibly obtained using methods such as optical reflectivity, X-ray reflectivity, or ellipsometry.^[10,31] The compliance of the PDMS substrate was obtained using conventional tensile testing.

The above results highlight another important aspect of the wrinkling technique, which is its amenability to performing thin-film modulus measurements in a high-throughput, combinatorial scheme.^[64,65] The data presented in **Figure 6** demonstrate the ease with which measurements can be rapidly performed on a sample with a variation in film thickness; one could easily imagine incorporating other types of 1D property gradients that would be extremely valuable for both research and product development purposes, or even 2D gradients in properties whereby two film properties gradients are constructed orthogonal to each other on the substrate surface. In the latter case, a 2D *phase space* of thin-film mechanical properties could be obtained simply by rastering around on the substrate surface and measuring the film thickness and wrinkling wavelength at each point of interest.

In order to demonstrate that the surface wrinkling technique would have the capability of measuring thin-film mechanical property changes arising from various mechanisms, NIST researchers investigated discrete samples of PS with varying amounts of dioctyl phthalate (DOP) plasticizer, and a series of organosilicate films with varying levels of porosity.^[10] In both cases, as shown in **Figure 7**, the measured modulus decreased predictably in response to increasing concentrations of plasticizer (**Figure 7a**) or porogen (**Figure 7b**) in the film. For the case of DOP in PS, the modulus followed the well-known sigmoidal trend as is likewise exhibited by materials such as poly(vinylchloride), and in the case of the porous organosilicate, the data could be fit to the model of Phani and Niyogi.^[66] In both cases, nanoindentation measurements (on thicker films) confirmed the accuracy of the surface wrinkling technique, the latter of which was superior in both the ease and speed with which the mechanical measurements could be performed.

Surface wrinkling has also proven quite flexible in the types of materials that can be tested and the modulus characterization range that is available to the technique. We have demonstrated,

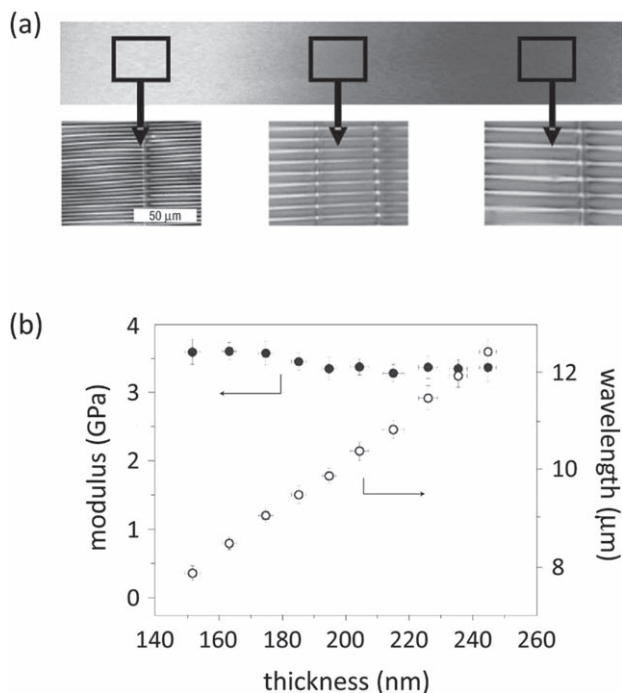


Figure 6. Young's modulus and wrinkling wavelength of PS as measured on a sample with a gradient in film thickness. a) Optical microscopy image of a PS gradient film showing the increase in wrinkling wavelength with film thickness. b) Young's modulus (closed circles) and wrinkling wavelength (open circles) for the gradient sample as calculated using Equation 13. The Young's modulus is constant with thickness over this range, varying little from its average value of 3.4 GPa \pm 0.1 GPa. A constant value for Young's modulus also implies the linear relationship observed between wavelength and film thickness. The error bars represent one standard deviation of the data, which is taken as the experimental uncertainty of the measurement. Reproduced with permission.^[10] Copyright 2004, Nature Publishing Group.

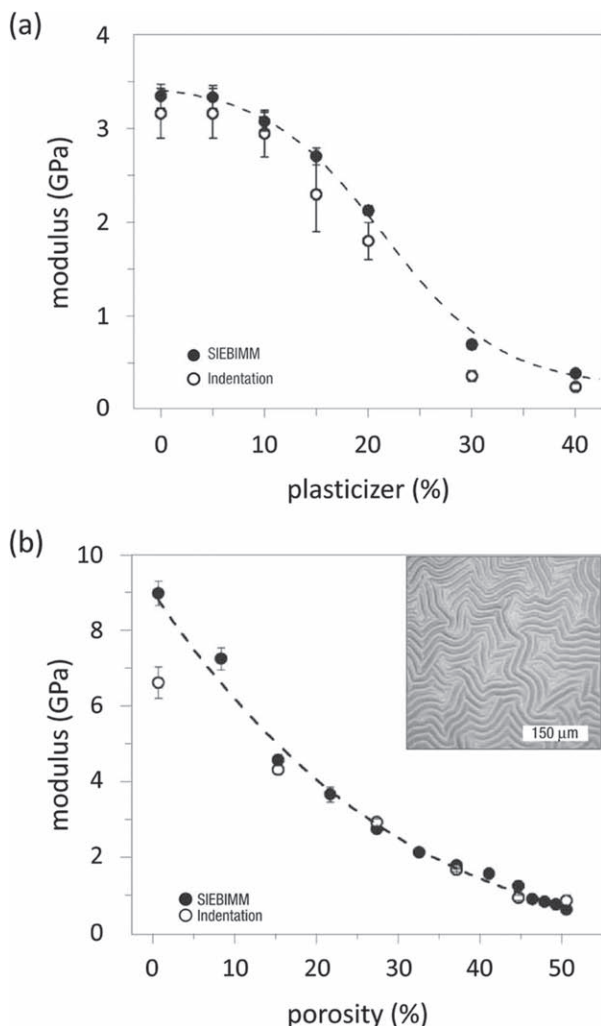


Figure 7. Young's modulus as a function of plasticizer and porogen content for PS and organosilicate films. The modulus in all samples was obtained using both surface wrinkling (closed circles) and nanoindentation (open circles). a) The Young's modulus of a series of PS films as a function of DOP mass fraction (%). The dashed line is a sigmoidal fit of the data, meant as a guide to the eye. b) The Young's modulus of a series of organosilicate films as a function of the volume fraction of air (porosity) in the film (%). The dashed line is the fit of the data using the model of Phani and Niyogi.^[66] The inset shows isotropic wrinkling in a porous organosilicate film. The error bars represent one standard deviation of the data, which is taken as the experimental uncertainty of the measurement. Reproduced with permission.^[10] Copyright 2004, Nature Publishing Group.

for example, that more compliant, elastomeric systems such as polystyrene-polyisoprene-polystyrene P(S-I-S) ($E \approx 100$ MPa) block copolymer films can be incorporated into a bilayer film with PS. By creating films comprising a P(S-I-S) film flow-coated on top of a PS film, each with a gradient in thickness, one can create a bilayer composite film structure that wrinkles with an effective modulus whose value depends on the relative thickness of the P(S-I-S) and PS layers at that point in the structure (see **Figure 8a**). The predicted effective modulus of such a composite film can be analytically calculated using standard plate mechanics, and is given by:^[31]

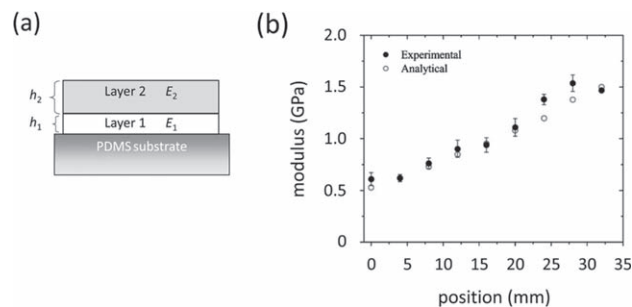


Figure 8. Wrinkling of a bilayer film. a) Schematic of a bilayer film, where two materials of different thicknesses and Young's moduli are stacked on top of one another. Such films undergo wrinkling at a wavelength that represents an *effective modulus* for the composite stack, which is a function of the relative ratios of the two layers' thicknesses and Young's moduli, as given by Equation 14. b) Young's modulus of a P(S-I-S) (layer 2)/PS (layer 1) bilayer film where each layer possessed a gradient in thickness. The effective Young's modulus values found for the composite film using wrinkling (closed circles) and those calculated using Equation 14 (open circles) were in excellent agreement. Testing the sample at increasing position along the gradient thus amounted to measuring the effective Young's modulus for decreasing values of the thickness ratio, $n = h_2/h_1$. The error bars represent one standard deviation of the data, which is taken as the experimental uncertainty of the measurement. Reproduced with permission.^[31] Copyright 2005, AIP.

$$E_{\text{eff}} = \frac{1 + m^2 n^4 + 2mn(2n^2 + 3n + 2)}{(1 + n)^3(1 + mn)} E_1 \quad (14)$$

where m is the modulus ratio, E_2/E_1 , and n is the thickness ratio, h_2/h_1 , of the two layers (with the subscripts 2 and 1 denoting the upper and lower layers, respectively). For the P(S-I-S)/PS bilayer film, the experimental effective modulus showed excellent agreement with the analytical prediction, as shown in **Figure 8b**.

3.2. LbL Films and Composites

Surface wrinkling of a composite two-layer film has already demonstrated utility in other fields, such as layer-by-layer (LbL) assembly. Recently, Nolte et al. demonstrated that in certain cases LbL assembled polyelectrolyte multilayer (PEM) films would assemble well on PDMS substrates only after a thin PS layer was first transferred to the PDMS surface and treated briefly to enhance its hydrophilicity.^[67] Surface wrinkling was then used to measure the effective modulus of the resulting PS-PEM composite film, from which the modulus of the PEM layer could be found. These researchers' work also expanded the range of materials that could be measured using surface wrinkling by demonstrating a practical method for modifying the wettability of the PDMS substrate through the use of a thin polymer layer that could be treated using plasma or ultraviolet/ozone (UVO) without the subsequent oxidation, damage, and hardening that would be expected upon treating the PDMS directly.

In fact, surface wrinkling proved to be of particular utility for LbL researchers, who previously had no straightforward and flexible method of obtaining Young's modulus values for these thin-film materials. Surface wrinkling has now been

used to probe the Young's modulus of a number of LbL materials, including porous and composite films comprising novel structures such as nanoparticles, nanowires, and carbon nanotubes.^[32,68–76] An additional benefit for the technique as applied to LbL materials is that surface wrinkling can easily be implemented in situ to examine the plasticization of films in aqueous solutions,^[34] as well as the response of films in air to changes in the relative humidity.^[77] In this way, surface wrinkling has helped uncover some previously unknown and interesting properties about LbL assemblies. For example, a recent study by Nolte et al. demonstrated that PEM assemblies comprising poly(allylamine hydrochloride) (PAH) and poly(acrylic acid) (PAA), which were previously known to be very hydrophilic, can in fact resist both swelling and plasticization by water at modest humidity values, transitioning abruptly at a relative humidity of $\approx 70\%$ to a highly swollen and low-modulus state.^[77] This abrupt transitional behavior, illustrated in **Figure 9**, is believed to be due the presence of a strong hydrogen-bonding network in PAH/PAA films assembled at low pH where many free carboxylic acid groups are present within the film.^[77] The discovery of this behavior was specifically enabled by the nature of the surface wrinkling technique and the ease and speed by which wrinkling wavelength measurements could be made using light scattering within the confined space of a humidity control chamber.

Wrinkling also offers significant advantages for characterizing LbL composites and heterogeneous materials. In regions where the instability wavelength is significantly larger than the heterogeneity length scale, surface wrinkling will yield an averaged, effective modulus for the system. As the instability length scale approaches the heterogeneity length scale, however, the wavelength will bifurcate and adopt different values to reflect local regions of higher or lower modulus. This fact has been demonstrated by Tsukruk and coworkers, who fabricated spin-assisted

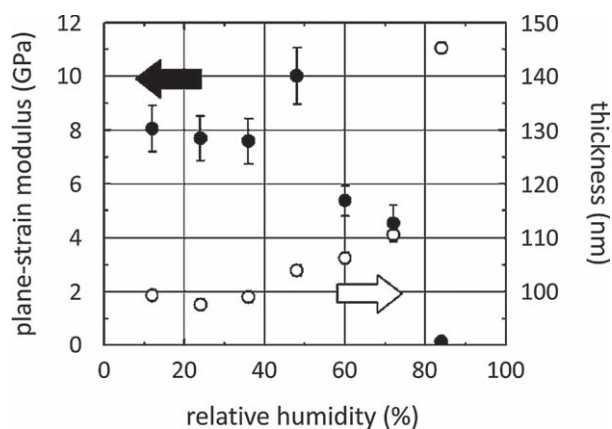


Figure 9. Plasticization and swelling of a LbL assembly as a function of relative humidity. The data were obtained from a polyelectrolyte multilayer film assembled on a PDMS substrate from PAH and PAA solutions at pH 2.5, which produced a film rich in free carboxylic acid groups. The plane-strain modulus (closed circles) and the film thickness (open circles) were obtained via wrinkling and spectroscopic ellipsometry, respectively, after equilibrating the film for ≈ 24 h at each humidity value. The error bars were calculated by propagation of estimated uncertainties in the wrinkling wavelength and film thickness measurements. Reproduced with permission.^[77] Copyright 2008, ACS.

LbL membranes embedded with microprinted arrays of gold nanoparticle stripes.^[32] When compressed, these membranes exhibited larger wavelengths in the nanoparticle regions due to local enhancement of the Young's modulus in those regions. Separate Young's modulus values could be calculated from the same sample for the LbL and LbL-nanoparticle composite regions (**Figure 10**). Because of the ease of measuring the directional dependence of mechanical properties in a thin film (by simply changing the direction of compressive forces), surface wrinkling also could be used to examine local orientation effects on modulus in liquid crystals, organogelators, and other self-organizing molecular systems.

3.3. Polymer Brushes and Hydrogel Substrates

Polymer brushes represent another interesting responsive thin-film system that has proven amenable to characterization via wrinkling.^[38,39] In a brush film, one end of each polymer chain is grafted to the substrate via a covalent bond, which toughens the film–substrate interface and prevents slip or delamination. Polymer brush layers on PDMS could serve a number of potentially useful roles to modify its friction and adhesion properties, as well as to enhance its biocompatibility. We have been successful at growing polymer brushes from PDMS surfaces that have been oxidized in a mild acid solution and reacted with a silane-bonded initiator in order to grow polymers via atom-transfer radical polymerization (ATRP).^[38] This technique produces polymer films on the PDMS surface with low polydispersity (and hence low roughness) and with a final thickness that is completely tunable by simply varying the polymerization time.

Surface wrinkling can play an important role in characterizing the properties of polymer brush layers on soft substrates such as PDMS. While techniques such as spectroscopic ellipsometry can be used to accurately determine the thickness of a thin polymer film on a transparent substrate such as PDMS,^[34,38] not everyone has access to such instruments and often a quicker and more straightforward approach to characterizing the brush thickness is desired. Furthermore, often a thickness measurement may be desired for a nonplanar substrate geometry, in which case ellipsometry would be an ill-suited technique. By examining a poly(2-hydroxyethyl methacrylate) (PHEMA) brush with a gradient in thickness, we have demonstrated that the grafting-from approach we have developed leads to brush layers whose mechanical stiffness does not vary as a function of thickness. The results for one sample with a gradient in brush thickness ranging from 25 to 70 nm are shown in **Figure 11**, where the average calculated modulus using surface wrinkling was $2.6 \text{ GPa} \pm 0.5 \text{ GPa}$, which is very close to the reported bulk modulus ($\approx 2 \text{ GPa}$) of this polymer.^[78]

The near-equivalence of the reported bulk modulus and the brush layer modulus allows wrinkling to be employed as a film thickness measurement tool. By inverting Equation 5, the thickness of the brush film can be expressed in terms of the wrinkling wavelength and the ratio of the moduli of the substrate and brush film as:

$$h = \frac{\lambda}{2\pi} \left(\frac{3\bar{E}_s}{\bar{E}_f} \right)^{\frac{1}{3}} \quad (15)$$

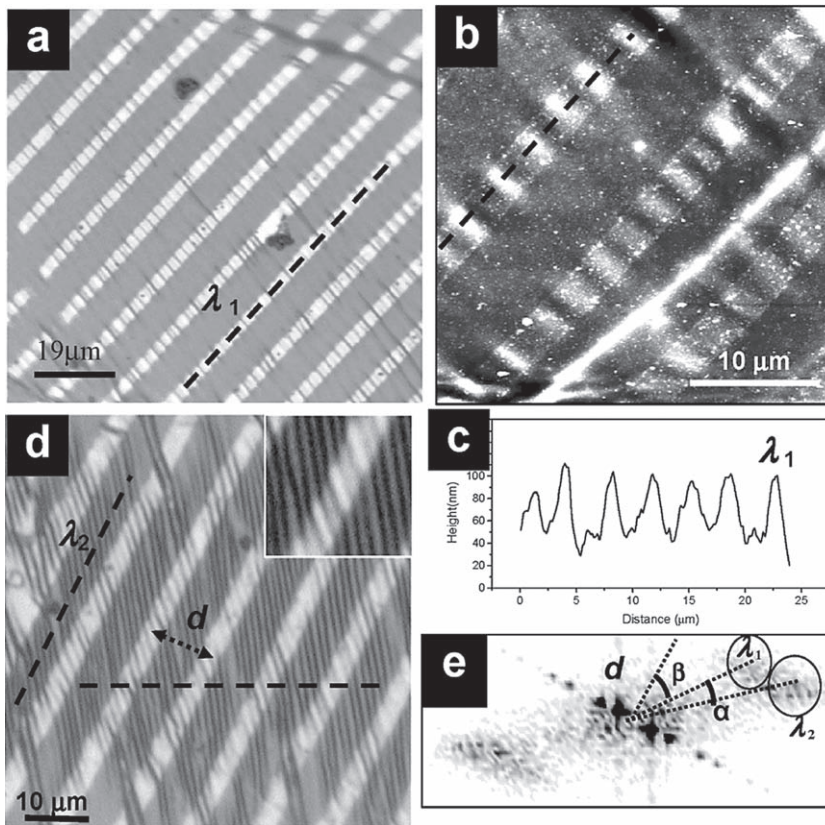


Figure 10. a) Optical and b) atomic force microscopy images of a micropatterned LbL composite film. The thin striped regions contain gold nanoparticles. c) A height profile along the dashed line shown in (a). d) At compressive strains greater than 0.3% distinct buckling modes can be seen in each region of the film, illustrated more closely in the $14 \mu\text{m} \times 14 \mu\text{m}$ inset. e) A Fourier transform image of striped composite film. Reproduced with permission.^[32] Copyright 2006, ACS.

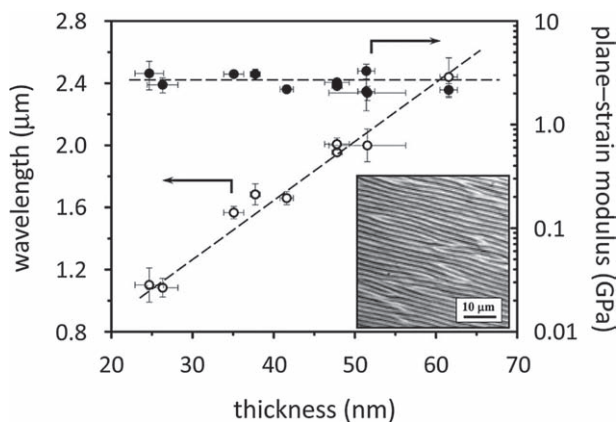


Figure 11. Plane-strain modulus and wrinkling wavelength of a gradient-thickness PHEMA brush grafted from PDMS. Consistent with the results presented in Figure 6, the wrinkling wavelength (open circles) increases linearly with brush layer thickness, indicating that the plane-strain modulus of the film (closed circles) is constant. The inset is an optical microscopy image of a wrinkled surface under uniaxial planar compression. The average Young's modulus for the PHEMA brush (assuming a Poisson's ratio $\nu_f = 0.33$) was $E_f = 2.6 \text{ GPa} \pm 0.5 \text{ GPa}$. The dashed lines are guides to the eye. The error bars represent one standard deviation of the data, which is taken as the experimental uncertainty of the measurement. Reproduced with permission.^[38] Copyright 2007, ACS.

Because E_s is well-known for PDMS and E_f is taken as the reported bulk value of the brush layer polymer, Equation 15 requires one to know only the wrinkling wavelength of a polymer brush in order to calculate its thickness. Thus, by multiplying the typically micrometer-scale, easy-to-measure wrinkling wavelength by the factor on the right-hand side of Equation 15, one can obtain the more difficult-to-measure thickness of the brush layer. We have demonstrated that this measurement method can be quite accurate for polymer brushes in the 10 to 100 nm thickness range.^[38]

Surface wrinkling of a thin film on a compliant foundation requires a modulus mismatch whereby the film Young's modulus must be, at a minimum, approximately an order of magnitude greater than that of the substrate. This imposes a practical limit on measuring the properties of thin, very compliant films, because substrates with modulus $E < 100 \text{ kPa}$ are difficult to handle and manipulate. A further development of the wrinkling technique at NIST, however, has significantly lowered the minimum modulus that can be measured by employing a thin film of a well-characterized polymer as a sensor film, and inverting Equation 13 to solve for the substrate modulus:

$$\bar{E}_s = \frac{\bar{E}_f}{3} \left(\frac{\lambda}{2\pi h} \right)^{-3} \quad (16)$$

The above approach presents an attractive method of obtaining the Young's modulus of very soft materials, such as biological hydrogels, as these experiments can be done in situ on hydrated samples, and the wrinkling measurements can still be performed on materials with gradients in properties, allowing for high-throughput characterization schemes with minimal additional effort.^[36]

To demonstrate this concept, 2-hydroxyethyl methacrylate (HEMA) solutions were prepared with cross-linker mass fractions ranging from 0.5% to 8% and deposited sequentially by syringe into a rectangular mold, with photopolymerization of the mixtures following each addition of new material.^[36] The resulting rectangular-shaped PHEMA hydrogel had a discrete gradient in mechanical properties, with HEMA solutions having greater cross-linker content giving rise to gels with higher Young's modulus values. PS films of approximately 100 nm thickness were used as sensor films due to their ease of fabrication and their well-characterized mechanical properties. These films were spin-coated from toluene solutions onto Si, and their thickness values were determined using optical reflectivity. The PS films were then floated from the Si wafer by immersion in water, after which the gradient modulus PHEMA gel could be gently used to pick up the sensor film. The PHEMA-PS sample was then immersed partially in water to keep it hydrated and it was compressed to

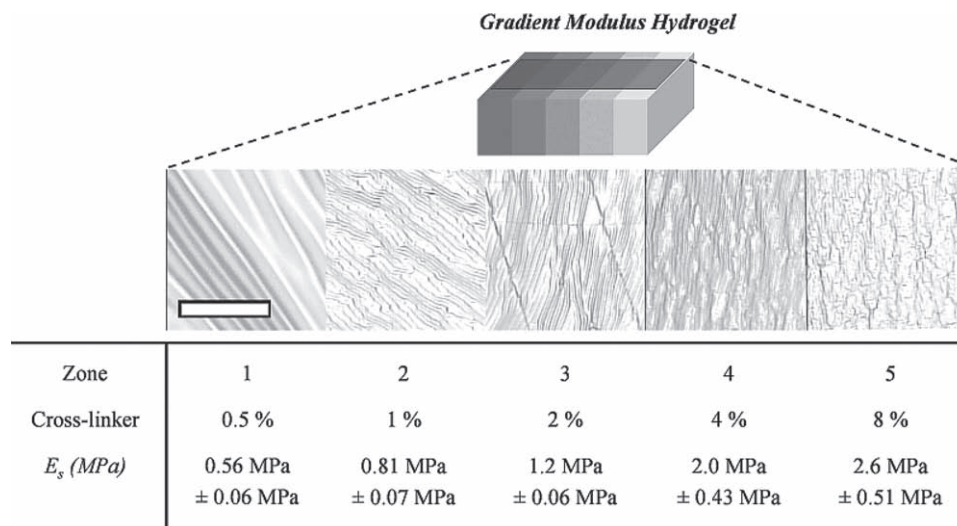


Figure 12. Measuring the modulus of a bulk hydrogel using surface wrinkling. The schematic depicts a sample with a discrete modulus gradient caused by polymerizing a PHEMA sample with different mass fractions (%) of cross-linker, as shown in the table. A PS film of known thickness and Young's modulus was wrinkled on the gradient sample, and the wrinkling wavelength from each modulus zone was found using optical microscopy (scale bar represents 100 μm). These data were used to solve for the unknown substrate modulus (E_s) using Equation 16. The measurement uncertainties represent one standard deviation of the data. Reproduced with permission.^[36] Copyright 2006, ACS.

induce wrinkling. Optical microscopy images of the wrinkled PS film from different points on the surface of the PHEMA hydrogel are shown along with the measured gel modulus in **Figure 12**.

Figure 12 illustrates the ease with which surface wrinkling can be implemented to probe the modulus at multiple points on the surface of a soft polymer gel; in this case, these points represented different formulations of monomer composition that gave rise to different modulus values in the resulting cured sample. The measured Young's moduli were in excellent agreement with parallel testing done by conventional compression tests on each monomer formulation.^[36] In the case of the gradient sample pictured in Figure 12, however, surface wrinkling enabled rapid characterization of multiple sample compositions in a fraction of the time such tests would have required using conventional techniques. These tests also demonstrated clearly that surface wrinkling could be successfully implemented as a metrology for soft hydrogel materials, which are currently of intense interest for a number of biomedical engineering applications (see for example the review articles by Hoffman^[79] and Peppas et al.^[80]). Recently, surface wrinkling has also been successfully applied at NIST to degradable tyrosine-derived polycarbonates, which are a class of polymers being investigated for biomedical applications such as arterial stents, hernia meshes, and drug-releasing coatings.^[81]

3.4. Nanoscale Systems and Confinement Effects

Interestingly, in addition to probing the mechanical properties of soft materials, wrinkling techniques have been implemented with equal success in examining some of the stiffest materials currently known. Rogers and coworkers utilized wrinkling to measure the Young's modulus of oriented single-walled carbon nanotubes (SWNTs) on a PDMS substrate.^[40,82] These

researchers' work demonstrated that for tubes with diameters in the range of 1 to 3 nm, the wavelength of wrinkling varied from approximately 100 to 300 nm and could be predicted using linear elasticity theory (**Figure 13**).^[40] Their calculations yielded a SWNT Young's modulus of 1.3 TPa \pm 0.2 TPa, which was in good agreement with previous atomic force measurements and first-principles calculations.^[40,82] The researchers also demonstrated that these materials could be implemented as a type of stretchy conductor with a strain-dependent resistivity, and suggested that their general techniques could be applicable to manipulating and characterizing other materials with similar dimensions, such as DNA. In addition, their work showed that wrinkling techniques were poised to help address cutting-edge challenges in nanoscience requiring innovative approaches to characterization.

One such challenge has been the determination of the stiffness of ultrathin (sub-100 nm) polymer films, which have been the focus of a considerable degree of interest due to the question of how nanoconfinement may affect their mechanical properties.^[83,84] Wrinkling has been used to demonstrate that the measured moduli of PS and PMMA films with thicknesses ranging from 5 to 200 nm begin to decrease when the film thickness is less than \approx 40 nm. This decrease in modulus can be substantial; for PS, the Young's modulus was observed to change almost an order of magnitude from the bulk value of $E \approx$ 3.6 GPa to \approx 500 MPa when the film thickness was decreased from 40 nm to 5 nm.^[30] Although the exact reason for this decrease remains uncertain, it was found that the data could be explained by postulating an effective two-layer model, where the film was treated as two separate layers (plates) wrinkling in unison using the mechanics approach discussed earlier.^[30,85] In such a model, the film is assumed to have two regions: a thicker layer with a modulus very close to the *bulk* (thick-film limit) modulus of the polymer (E_f), and a thinner *surface layer*

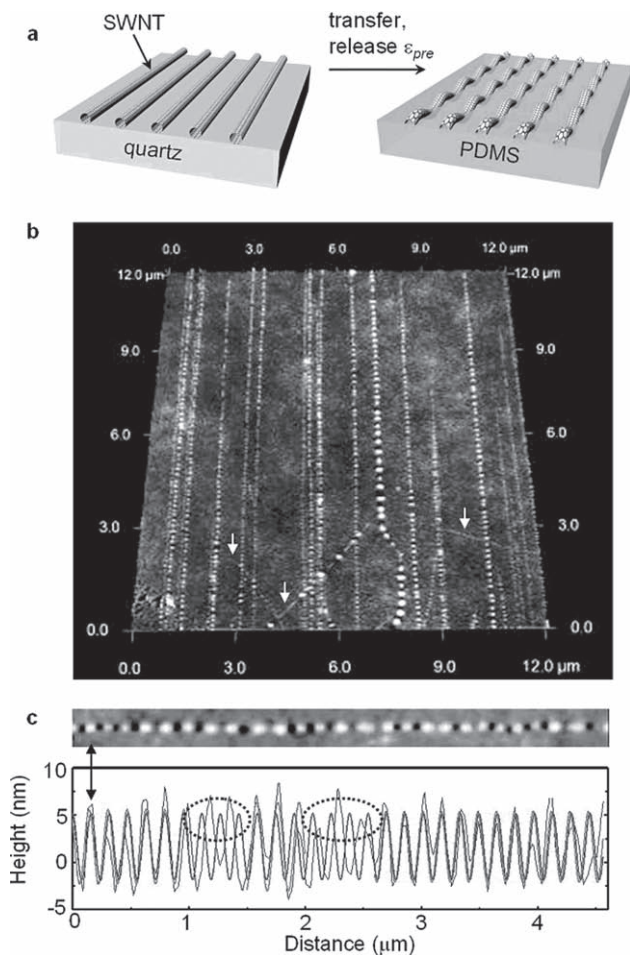


Figure 13. a) Transfer of aligned arrays of SWNTs grown on quartz to a uniaxially strained substrate of PDMS followed by release of the prestrain (ϵ_{pre}) causes nonlinear buckling instabilities in the SWNT that lead to wavy configurations. b) Large-area ($12 \mu\text{m} \times 12 \mu\text{m}$) angled-view AFM image of wavy SWNTs on a PDMS substrate. c) Plane-view AFM image of an individual wavy SWNT and linecut showing the profile of relief. A detailed explanation on this height profile can be found in.^[40] The wavelength determined by the piecewise fit is $160 \text{ nm} \pm 20 \text{ nm}$. Reproduced with permission.^[40] Copyright 2008, ACS.

(with thickness δ) that has a lower modulus (\bar{E}_f^*) reflective of the increased mobility of polymer chains near a free interface. Assuming the wrinkling data represented the effective modulus (\bar{E}_{eff}) of the film, and treating the Young's modulus of each individual layer and the thickness of the surface layer as fitting parameters in Equation 14, very good fits of the data were obtained. The data and fit curve for PS are shown in **Figure 14**.

The best fit curve for the PS data in Figure 14 was obtained when $\bar{E}_f = 3.7 \text{ GPa}$, $\bar{E}_f^* = 0.089 \text{ GPa}$, and $\delta = 2 \text{ nm}$. Similar results were obtained for PMMA. Overall, the results of this work suggested that the apparent mechanical stiffness of amorphous polymers can decrease substantially below a critical thickness of $\approx 40 \text{ nm}$,^[30] a finding which is in good agreement with the predictions of previous simulations by de Pablo and coworkers.^[86,87] This work also demonstrated that wrinkling was well-suited to address questions of how the properties of

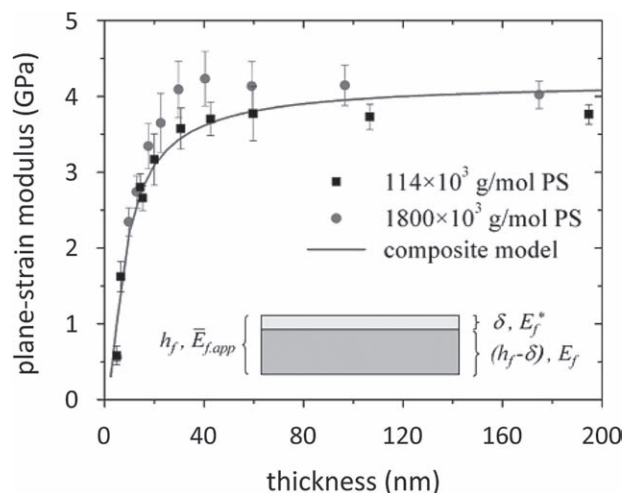


Figure 14. Plane-strain Young's modulus for PS films of different molecular weight as a function of film thickness. The solid line is a fit for a composite model having $\bar{E}_f = 3.7 \text{ GPa}$, $\bar{E}_f^* = 0.089 \text{ GPa}$, and $\delta = 2 \text{ nm}$. The error bars represent one standard deviation of the data, which is taken as the experimental uncertainty of the measurement. Reproduced with permission.^[30] Copyright 2006, ACS.

ultrathin materials respond to ever-shrinking dimension sizes. Indeed, we have further explored the impact of quench depth (i.e., how far the measurement temperature is from the glass transition temperature) on the mechanical properties of confined polymer thin films.^[33] In that study, a strong correlation was found between the thickness of the free surface layer (δ) and the quench depth for a series of methacrylate polymers. This topic is of great importance for the continued development of nanotechnological application, particularly as it pertains to fields such as lithography where increasing mechanical demands are put on polymer nanostructures as semiconductor device sizes approach the molecular scale.

The past two decades have seen an explosion of interest in surface instability phenomena, particularly as applied to the types of metrology applications detailed in this section. **Figure 15** illustrates the phenomenal range of applicability of wrinkling-based techniques that have been applied to a range of materials whose Young's modulus values span seven orders of magnitude. With continuing interest in the development of new materials and techniques to rapidly screen their properties, surface wrinkling should provide a convenient method for materials scientists to examine thin films and soft materials in an effort to better understand their mechanical properties and how such properties relate to the materials' structure and dimensions.

4. Beyond Modulus Measurements

Over the past several years, researchers have made significant progress in understanding and measuring wrinkling instabilities, focusing not only on characterizing the parameters of a post-wrinkled system, but also on examining the *dynamics* of wrinkling initiation and growth. Examining the dynamic onset of instabilities using quantitative analytical tools has provided

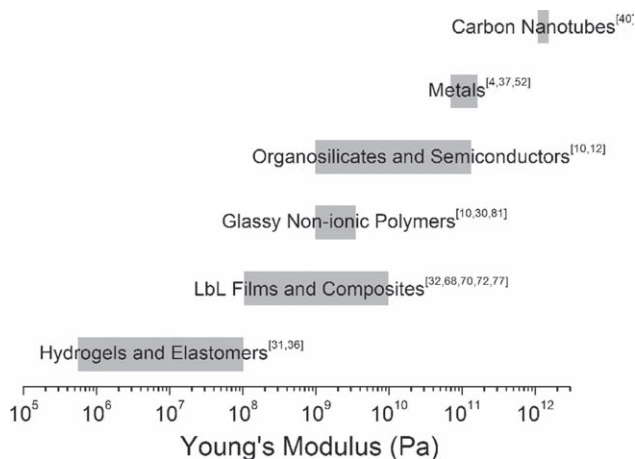


Figure 15. Range of Young's modulus values measured using surface wrinkling techniques as reported in the literature. References are given for each case to provide examples of work that has been performed, and are not meant to be exhaustive of all work in the respective fields.

new perspectives on how surface wrinkling may be employed as a metrology tool for applications beyond the thin-film modulus measurements discussed earlier. In the following section, we review recent progress in the development of surface wrinkling for advanced metrology applications. In so doing, we illustrate how surface wrinkling is poised to address a variety of complex measurement needs for thin films, and how the technique may be leveraged to dynamically change the properties of a surface for advanced materials science systems. We first illustrate how careful monitoring of wrinkle formation and growth can give added information about a film and how it reacts to external stimuli such as heat and solvent exposure. Secondly, we will discuss how reversible surface wrinkling may be leveraged in topology-sensitive phenomena such as wetting and adhesion.

4.1. Surface Force Sensing

Since the pioneering work of Whitesides and coworkers,^[4–6] surface instability-induced patterning of thin films has been a topic of extreme interest. Surface wrinkling is particularly interesting since its morphological surface configurations are associated with the stress fields evoked by the specific stimuli used to generate compressive stress in the film; this could be mechanical,

chemical, heat, light, electricity, etc. In all cases, the wrinkle orientation and amplitude ($A \sim \epsilon^{1/2}$) provide an immediate visual representation of both the direction and magnitude of stress induced within the system (**Figure 16**).^[7,14,15,17,57,59,61,88–94] This can be demonstrated, for example, by simply bunching together skin between ones fingertips: wrinkles develop locally normal to the applied direction of compression and their dimensions (local amplitude and propagation length) grow in proportion to the force exerted. The high sensitivity and specific growth characteristics of the wrinkling morphology make it possible to use such instability behavior as a sensitive indicator of stress response to external stimuli.

Perhaps the first promising attempt along the above lines was made in the 1980s and 1990s by Harris et al.^[95] and later by Burton and coworkers,^[96,97] who demonstrated the use of elastic distortion and wrinkling as a quantitative means of probing the traction force that a cell generates on a surface. In their work, tissue cells such as fibroblasts and keratocytes were cultured on flexible rubber films made by cross-linking a silicone fluid using a flame. Adherent cells caused surface wrinkles as they exerted forces on the substrates during their crawling locomotion (**Figure 17**). The relative magnitude of the traction force exerted by the cell was found to strongly correlate with the size of the wrinkles formed, which were compared to those generated by a pulled micro-needle that had been force-calibrated. This seminal work demonstrated that surface wrinkling could be utilized to visualize cell–substrate mechanical interactions. The concept of wrinkle force sensor has since opened up new avenues for research in fundamental cell biology, as the cell contractile force plays an essential role in cell migration, adhesion, and maintenance of cell shape.^[98] Recent reports have also suggested that the wrinkles themselves may be used to directly control the shape and orientation of cells grown on culture surfaces patterned using instabilities. More information and illustrative examples can be found in the literature.^[99,100]

We^[15] and others^[101] have also been using wrinkling to quantify the kinetics of solvent diffusion within polymeric thin films. In these studies, surface wrinkling patterns were observed on thin high-modulus films on compliant substrates (Ti-capped^[101] or UVO-treated^[15] PS films) as a result of osmotically driven swelling associated with the selective sorption of toluene vapor. In situ observation revealed that such wrinkle patterns occur at defects in the film surface and spread over large areas in response to swelling and film plasticization due to the local influx of solvent vapor; this behavior resembles the self-organized

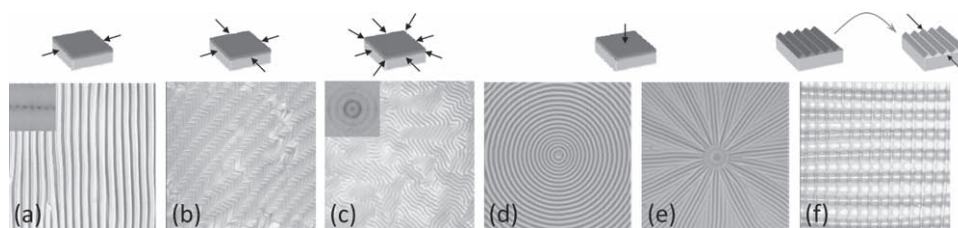


Figure 16. Optical images of various morphological patterns, demonstrating that the wrinkling patterns prefer to orient themselves perpendicular to the axis of principal compressive stress: a) stripes (uniaxial mechanical compression), b) herringbones (biaxial mechanical compression), c) labyrinths (isotropic thermal contraction),^[17] d,e) targets and spokes, respectively (solvent swelling at a local defect),^[15] and f) checkerboards (uniaxial mechanical compression on a prepatterned substrate). Panel c reproduced with permission.^[17] Copyright 2007, AIP. Panels d,e reproduced with permission.^[15] Copyright 2009, Wiley-VCH.

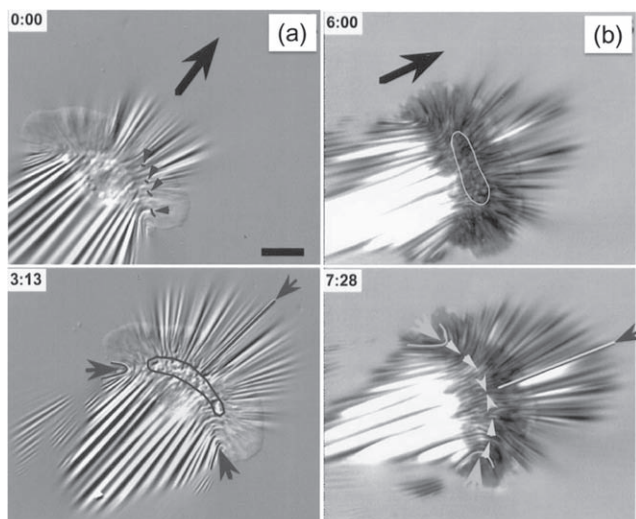


Figure 17. Deformation of a highly compliant substrate. a–b) Nomarski differential interference microscopy and interference reflection microscopy images of one keratocyte on a highly compliant substratum. Outlined areas under the cell body show where the silicone rubber was crinkled, obscuring wrinkles that were otherwise present (compare times 6 min and 7 min 28 s in (b)). Wrinkles were out of focus under the cell body in (a). Arrowheads in (a) (time 0:00) point to wrinkles and distortions that exhibited small inward lateral displacements (durations, 17 to 26 s). Arrowheads in (b) (time 7:28) indicate the positions and directions of forces that produced compression wrinkles centered near the boundary of the cell body and the lamellipodium. Force was symmetrical about the midline, where wrinkle curvature reversed (pair of angled arrowheads). Small arrows in (a) and (b) point to wrinkles used to estimate traction force (left, middle, and right): 120, 600, and 130 nN in (a) and 150, 700, and 146 nN in (b). Reproduced with permission.^[97] Copyright 1999, ASCB.

growth observed in many physical, chemical, and biological systems.^[102] Controlling the location and solvent diffusion rate into such films was shown to yield an incredible degree of control over the fidelity and morphology of the resulting patterns. In particular, we demonstrated that restricting the solvent influx into the film leads to a transition from Fickian to Case II diffusion behavior,^[103,104] with a concurrent change in wrinkle alignment from spoke-like patterns to concentric rings, as shown in **Figure 18**.^[15] By analyzing pattern growth kinetics and the stress fields in each diffusion regime, this work provided compelling evidence of the inherent connection between diffusion kinetics and pattern morphology. Furthermore, it was shown that the dynamics of wrinkling growth could be used to directly measure the diffusion coefficient of solvent within the film; it is our expectation that these findings will spark creative approaches to further understand and utilize these exciting phenomena.

4.2. Polymer Dynamics

The response of surface wrinkling to an instantaneous change in the thermal field also raises the interesting possibility of quantifying the thermomechanical behavior of polymer films. Lee and coworkers demonstrated that a polymeric thin film

capped with a thin metal layer (deposited by thermal evaporation) undergoes a wrinkling instability when heated above the glass-transition temperature (T_g) of the polymer.^[105–107] This instability occurs as a result of stress fields arising due to mismatches in the coefficients of thermal expansion (CTE) of materials in the system. The dynamics of this wrinkling process were shown to be driven in large part by temperature-dependent properties of the underlying polymer film, thus leading to a complex morphological diagram.^[107] Moreover, unlike the elastic wrinkling behavior described above previously, the thermally-induced viscoelastic wrinkling on the metal-polymer bilayer is time-dependent (here, wrinkle amplitude grows exponentially with time), in agreement with theoretical analysis.^[53] A recent study addressed this issue systematically through SALS analysis; SALS allows one to track the time-dependent evolution of wrinkling wavelength and amplitude as a function of annealing temperature (**Figure 19**).^[62] This study indicated that the real-time observations of thermally induced wrinkling could provide measurements of the viscoelastic properties (e.g., rubbery modulus and viscosity) of the polymer film by probing the isothermal time evolution of wrinkling growth. Moreover, this approach based on thermal wrinkling can also be extended to materials that undergo other thermal phase transitions, such as order-disorder transitions. Steps towards experimental measurement of the rubbery modulus and shear viscosity of a variety of confined polymer systems, including polymer brushes, polymer nanocomposite thin films, and block copolymers, are currently under way.

The onset of surface wrinkling has also been examined for measurements of the residual stress in polymer films that arise as a consequence of film formation via techniques such as spin casting. We have recently demonstrated that such stresses can be quantified by measuring the critical strain for the onset of wrinkling.^[61] Solvent-cast polymer films, which are found in numerous coatings applications, generally contain a number of polymer chains kinetically trapped in non-equilibrium conformations, giving rise to a residual stress state in the film.^[108] The measurement and control of residual stress is of increasing relevance as polymer structures shrink in size and are incorporated into defect intolerant applications, such as nano or micro-mechanical, -electronic, -magnetic, and -optical devices. Moreover, predictive routes to anticipating the presence of residual stress and the impact of steps taken to remove it are currently of limited value given the complexity of such calculations and the number of factors that must be accounted for in considering any one film fabrication technique.^[109] Conventional techniques, such as wafer curvature and cantilever deflection-based methods, are particularly challenged by polymeric thin films, due to their limited resolution and sensitivity for resolving the relatively small changes in deformation caused by soft materials.^[110]

To overcome these difficulties, we have utilized compression-induced wrinkling of a thin polymer film attached to a soft substrate, where the periodic wrinkling wavelength and the onset of wrinkling yield the theoretical critical strain (ϵ_{c0} , Equation 7) and observed critical strain (ϵ_c) for thin film wrinkling, respectively.^[61] In the presence of residual strain (or stress), the relationship between residual strain ($\epsilon_R = \epsilon_c - \epsilon_{c0}$) and residual stress (σ_R) is given by $\sigma_R = \bar{E}_f \epsilon_R$ (note that $\epsilon_c \approx \epsilon_{c0}$ when residual

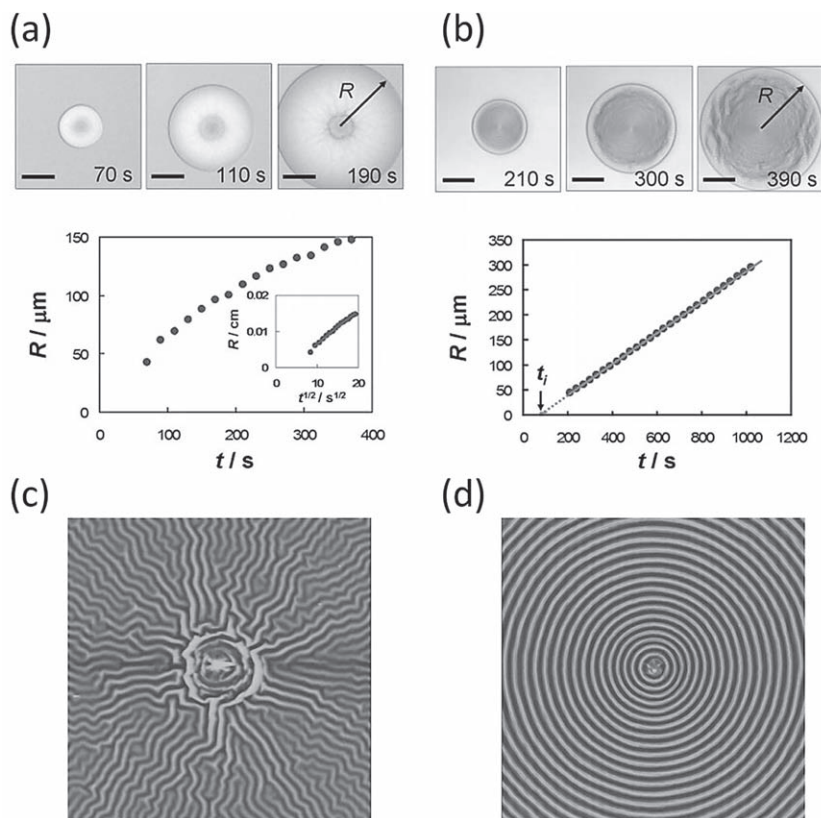


Figure 18. A sequence of snapshots of the time evolution of spoke and target patterns formed on a 500 nm-thick PS film. These patterns initially nucleated at randomly distributed defect sites and then expanded to a size readily visible to the eye. a) Spoke pattern. t_{UVO} (UVO exposure time) = 3 min. The plot shows the radius of the wrinkled front (R) versus elapsed time (t). R was replotted against $t^{1/2}$ (inset) and fitted with a linear regression line, showing that the data collapse on a single line given by $R \approx 9.4 \times 10^{-4} t^{1/2}$. b) Target pattern. $t_{\text{UVO}} = 10$ min. The plot shows that R increases linearly with t , and the solid line is the best fit with $R \approx 0.32 t - 23.6$. From the data, the growth velocity of target pattern was found to be $V \approx 0.3 \mu\text{m s}^{-1}$. The nonzero horizontal intercept corresponds to the induction time ($t_i \approx 80$ s) required for pattern initiation, the existence of which is known as a typical characteristic of Case II diffusion.^[103] Scale bars in (a) and (b) are 30 μm . c) AFM height image (50 $\mu\text{m} \times 50 \mu\text{m}$) of the spoke pattern produced on a 500 nm-thick PS film with $t_{\text{UVO}} = 3$ min. d) AFM height image (50 $\mu\text{m} \times 50 \mu\text{m}$) of the target pattern comprising a series of concentric rings formed on a 500 nm-thick PS film after $t_{\text{UVO}} = 5$ min. Reproduced with permission.^[15] Copyright 2009, Wiley-VCH.

stress is absent or negligibly small). Thus, the unknown residual stress in the film can be extracted by measuring the strain necessary to induce wrinkling (ϵ_c) and the wrinkling wavelength, which yields \bar{E}_f (Equation 13) and thus ϵ_{c0} (Equation 7). The capability of this metrology was validated with spin-cast, thin (20 to 400 nm) PS films, which were initially deposited on smooth substrates (e.g., silicon, mica). The films were then transferred onto PDMS substrates, and the critical strain and wavelength of wrinkling were measured using SALS to determine the residual stress (see **Figure 20a–b**; note that thin (>100 nm) PS films prepared via spin casting possess residual stresses of ≈ 30 MPa). This wrinkling-based residual stress measurement is especially well-suited for testing nanoscale thin films; in contrast to the classical wafer-curvature method, surface wrinkling does not require any specialized equipment and is less prone to experimental error because the threshold strain can be precisely measured, allowing for high enough resolution

to measure residual stress in ultrathin (sub-100 nm) polymer films (Figure 20c).^[61] This approach was successfully applied in case studies involving two widely used strategies for the dissipation of residual stress in polymeric thin film (thermal annealing and plasticizer addition), and provided qualitative insight into stress relaxation mechanisms (for example, see Figure 20d).

4.3. Surface Property Control

The use of wrinkling to produce and control surface morphology has also been an area of interest for us and other researchers. Surfaces that possess topographical patterns have long been recognized as an effective means for controlling surface properties such as adhesion, wetting, friction, and cell attachment. Motivated by unique, topology-controlled properties found in nature, such as the self-cleaning effect of lotus leaves^[111,112] and the remarkable adhesive ability of geckos^[113] and some insects,^[114] current efforts have been directed towards designing smart materials with properties targeted for specific applications.^[115–117] To fully understand the role that surface topography plays in various interfacial phenomena, researchers have been searching for ways to fabricate surfaces with well-defined pattern geometries. In this respect, the wrinkling-based technique is particularly appealing since regularly ordered patterns can be easily generated in a scalable and cost-efficient manner over large surface areas. In addition, such patterns are tunable; compression and relaxation of the sample is often sufficient to tune the pattern aspect ratio or even erase it completely.^[12,38,118,119] Wrinkle control by other types of stimuli is also possible; for example, because they are covalently

bound to the PDMS surface, immersing a polymer brush in a compatible solvent plasticizes the film and erases the wrinkle pattern.^[38] By alternating thermal cycling of a PHEMA brush layer with rinses in a compatible solvent, we have demonstrated how the surface of a polymer brush on PDMS can be reversibly switched between wrinkled and flat topologies (**Figure 21**). The unique ability to dynamically tune the surface morphology affords wrinkling a significant advantage over the conventional lithographic methods, making it attractive as a potential tool for studying topography-driven phenomena.^[99,100,119–126]

Several recent studies have utilized surface wrinkling to explore various interfacial phenomena.^[99,100,119–122,126] In these studies, wrinkled surfaces were fabricated by mechanically stretching a PDMS slab uniaxially to a given prestrain (ϵ_0) and then oxidizing its surface with UVO radiation or an oxygen plasma for an extended period of time, which generates a silicate-like layer on its top surface. Upon releasing the initial

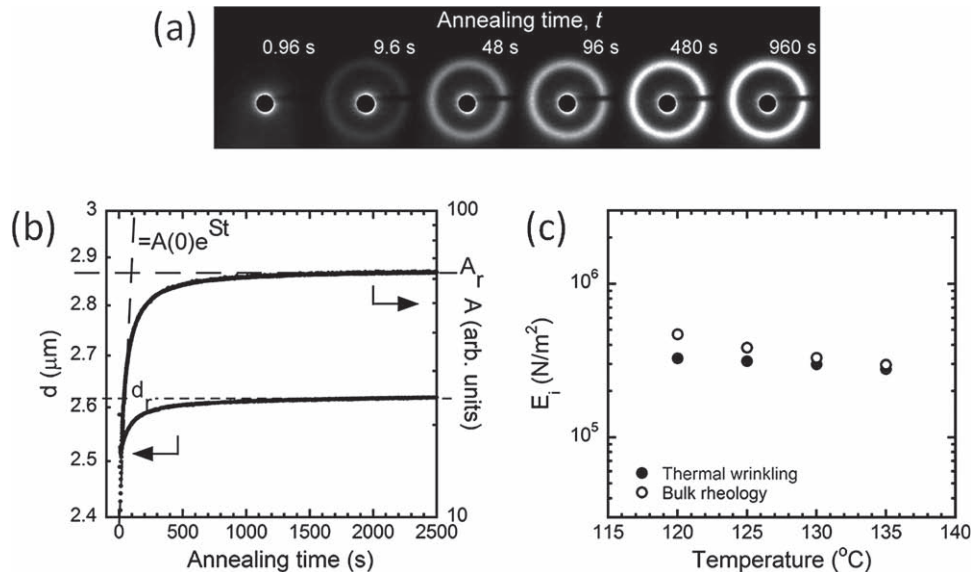


Figure 19. Representative data from thermal wrinkling of a polystyrene-aluminum bilayer for measuring the rubbery modulus of thin polymer films. a) Time-resolved small angle light scattering showing the evolution of the scattering intensity as a function of time. b) Evolution of both the wavelength (d) and the amplitude (A) of the surface wrinkling pattern, as extracted from the position and intensity of the time-resolved scattering shown in (a). c) The rubbery modulus, E_r , as a function of temperature deduced from the thermal wrinkling experiments as well as from conventional bulk rheology of a bulk specimen. Reproduced with permission.^[62] Copyright 2009, RSC.

ϵ_0 to the critical strain for onset of wrinkling (ϵ_c), a sinusoidally wrinkled 1D pattern formed perpendicular to the direction of the strain. Releasing the initial ϵ_0 beyond ϵ_c in turn increases the amplitude of these wrinkles according to Equation 11 (see also Figure 3), allowing for control of the pattern height. In addition, this method allows for tuning the wavelength of the pattern by adjusting exposure dose, which affects both the thickness and Young's modulus of the silicate layer as is evident from Equation 5. Moreover, the surface patterns can be erased by stretching the sample back to ϵ_0 (this recovery has been demonstrated on PDMS for values of the prestrain up to at least $\epsilon_0 \approx 50\%$).^[119] Because of these unique features, a precise and reversible control of patterned surface structures with a well-defined roughness aspect ratio ($A/\lambda \sim (\epsilon - \epsilon_c)^{1/2}$) becomes possible.

We have demonstrated the wetting behaviors on controlled wrinkle surfaces by contact angle measurements in two directions: perpendicular (θ_\perp) and parallel (θ_\parallel) to the direction of the grooves.^[119] Figure 22 shows the static water contact angle (CA) on tunable micro-wrinkled surfaces whose roughness aspect ratios were well-defined and reversibly adjustable. It is evident that the anisotropic surface morphology of a sinusoidally wrinkled 1D pattern can govern the wetting behavior, leading to different values for θ_\perp and θ_\parallel and a noncircular drop footprint. This directional dependence of the contact angle on a rough surface is significantly affected by the nature of the three-phase contact line structure. Recently, Lin and Yang^[120] extended the above-mentioned study by incorporating nanoparticles on a wrinkled PDMS film, and demonstrated the possibility of promoting the wetting transition from a Wenzel mode into a Cassie mode using a surface with dual-scale roughness. In their work, surfaces that possess dual-scale roughness were prepared with the

dip-coating of silica nanoparticles (diameter ≈ 100 nm) onto a pre-stretched (ϵ_0) and oxygen plasma-treated PDMS film. Upon wrinkling, microscale roughness features arose along with the nanostructure due to the particles; when the sample was stretched back to the initial ϵ_0 , only the nanoscale roughness remained. The researchers investigated the wetting behavior of their tunable wrinkled surfaces by performing CA measurements, and demonstrated that the surface with dual roughness became superhydrophobic with a CA $\approx 150^\circ$ (Cassie mode), whereas a surface with only a single-scale of roughness exhibited CA $\approx 62^\circ$ (Wenzel mode).

Along similar lines, Chan et al. demonstrated an elegant strategy for a reusable smart adhesive using surface wrinkling.^[123] In their work, highly structured, isotropic wrinkle patterns were generated by solvent swelling of a laterally confined and elastomeric poly(*n*-butyl acrylate) film. They prepared wrinkled surfaces with varying degrees of roughness by controlling the film thickness to study adhesion behavior. Contact adhesion tests revealed that the adhesion could be tailored by employing wrinkle patterns of specific wavelengths; the surface with the smallest wavelength exhibited a threefold greater adhesion than the surface with the largest wavelength. Additionally, they identified a possible mechanism known as contact splitting to explain improved control of adhesion, and provided a simple design principle to create a smart adhesive. Another approach was followed by Lin et al.,^[121] who demonstrated that a wrinkled surface with a highly ordered structure could be beneficial for systematically studying adhesion behavior. They utilized the tunability of wrinkle patterns that were fabricated through surface oxidation on a PDMS strip to explore a new mechanism for regulating adhesion (Figure 23a–i). By performing pull-off force measurements (microindentation) on the sample as a function

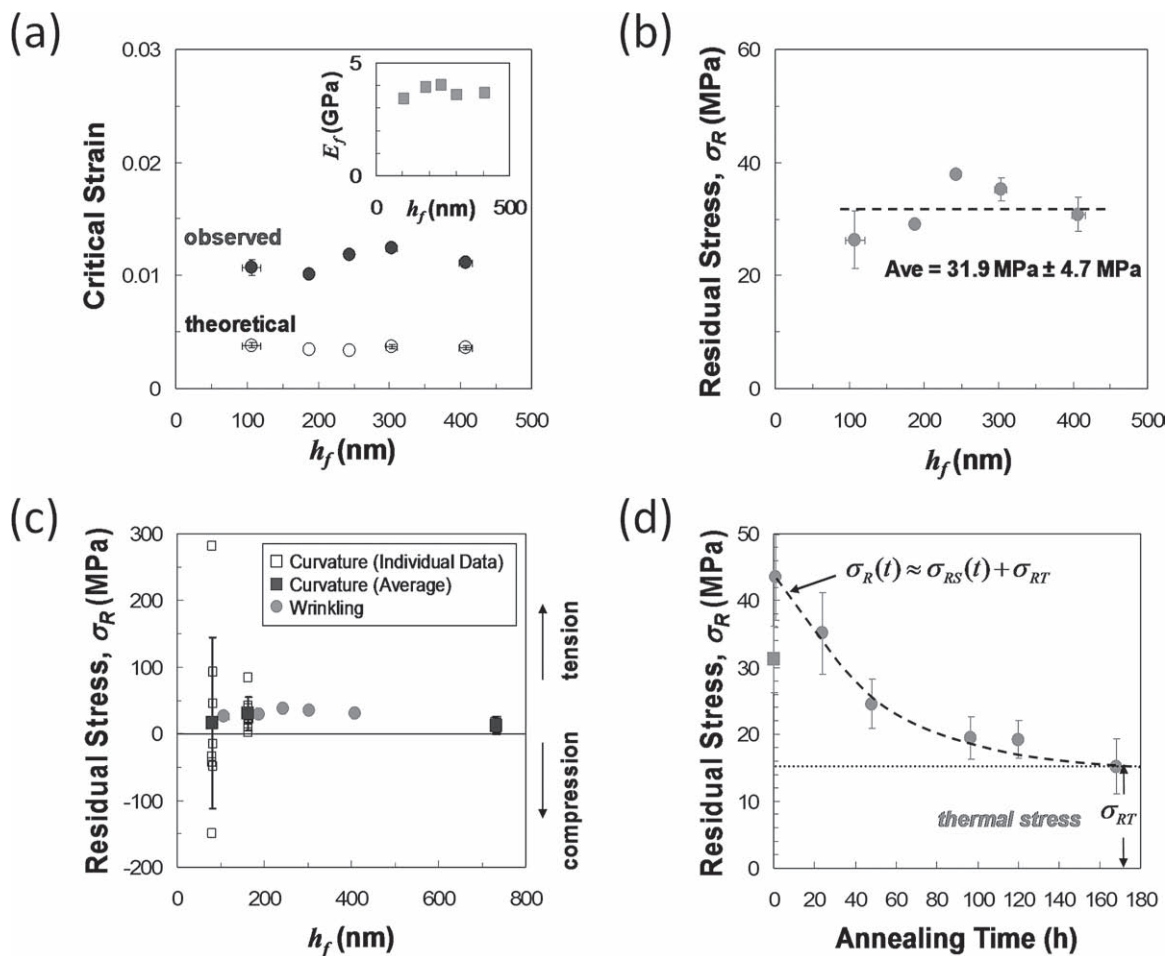


Figure 20. a) Observed critical strain (closed circles) and theoretical critical strain (open circles) obtained as a function of film thickness (h_f). The inset displays the measured modulus (E_f) as a function of h_f , which was calculated by means of Equation 13 using the measured wavelength (assuming $\nu_f = 0.33$). b) Corresponding residual stresses (σ_R) as a function of h_f . c) Residual stresses (σ_R) as a function of film thickness (h_f) measured by the wafer curvature-based technique. Open squares represent a single measurement. Closed squares are the average values obtained from at least eight individual measurements with the same thickness, and the error bars indicate the relative standard uncertainty of the mean of the measurements. Closed circles represent the residual stresses measured by the wrinkling method, which were reproduced from (b) for comparison. d) Residual stresses (σ_R) in PS films spin-coated onto mica substrates as a function of the annealing time, which ranged from 1 to 168 h. In all experiments, the film thickness was kept at $h_f \approx 120$ nm. The measured residual stress at a given annealing time, $\sigma_R(t)$, can be decoupled into two terms: stress induced by spin coating, $\sigma_{RS}(t)$, which decreases and asymptotically approaches zero as the annealing time increases, and a constant thermal stress, σ_{RT} , associated with cooling the sample down to room temperature after annealing. The square symbol represents the residual stress in PS films spin-coated onto mica substrates without annealing. In (b) and (d), the dashed lines are added to guide the eye and the error bars represent one standard deviation of the data, which is taken as the experimental uncertainty of the measurement. Reproduced with permission.^[61] Copyright 2009, ACS.

of planar strain (and hence wrinkle height), they discovered a significant and systematic decrease in adhesion with the increase in strain (Figure 23j–l). They further provided theoretical predictions based on contact mechanics models of two limiting cases involving low and high amplitude. Their study showed that such predictions agree well with the experimental results.

5. Conclusions and Outlook

This Review has provided an illustrative glance at the field of elastic surface instabilities, highlighting areas in which surface wrinkling instabilities in particular have been utilized to

characterize and tune the properties of materials and surfaces. One remarkable aspect of the current popularity of instability research is that such phenomena have been known and studied for hundreds of years, but generally with a desire to prevent their onset in engineering materials. While civil engineers will continue to design bridges and buildings to specifications that avoid mechanical buckling instabilities in columns and struts, materials and surface scientists have found that intentionally inducing these phenomena can be quite useful in a variety of applications. Future work within the field of surface wrinkling instabilities will likely be classified into two main categories: 1) metrology and characterization and 2) patterning and surface property manipulation.

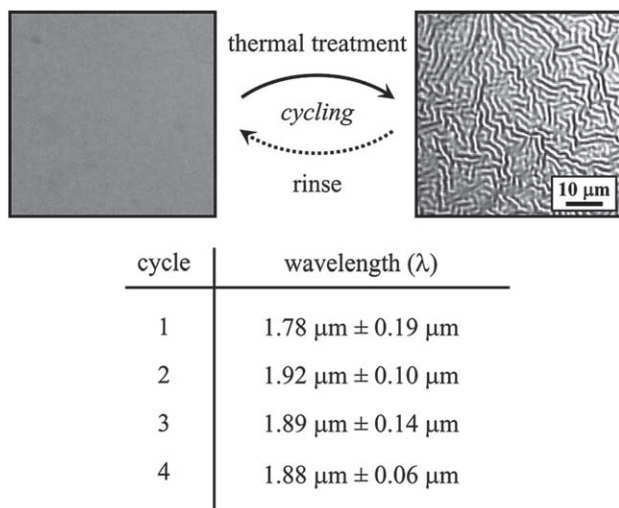


Figure 21. Reversible surface patterning using a PHEMA brush grafted from PDMS. Upon heating the sample above the T_g of PHEMA and cooling back to room temperature, an isotropic wrinkling pattern forms due to the thermal contraction of the PDMS. Upon rinsing the sample in a good solvent (e.g., water, ethanol, dimethylformamide, etc.), stresses in the brush layer are relaxed and the wrinkling pattern is erased. The process can be cycled multiple times with no statistically significant change in the wrinkling wavelength, as shown in the table. The measurement uncertainties represent one standard deviation of the data. Reproduced with permission from.^[38] Copyright 2007, ACS.

Instability-based measurement tools are well-suited to meet many future measurement challenges in materials science. With regard to the characterization of mechanical properties such as Young's modulus, instability patterns offer a distinct advantage in that the particular material parameter can be directly calculated from the feature length scale in a spontaneously formed pattern without employing a constitutive relation such as Hooke's Law. Practically speaking, this means that the

Young's modulus is reflected directly in the response of the material without the need to generate a controlled stress-strain curve, which would require additional tools to measure displacements and force. For characterization of nanoscale materials, this can offer significant advantages. Nanoscale-sensitive force and displacement sensors (such as those incorporated in AFMs or nanoindentors) are often quite expensive, and indentation distance measurements on the thinnest films can contain an unacceptable degree of experimental error. Surface wrinkling techniques can overcome these hurdles, and even allow for property measurements on nanostructures that are confined in multiple dimensions, such as a thin strip of lithographically patterned photoresist. In addition, samples can easily be characterized in space-restricted and nonambient environments; for example, straightforward measurements have been demonstrated in solution^[34] and in solvent chambers.^[15,77] The ability to easily conduct such measurements will be a key part of developing new materials for increasingly sophisticated and challenging applications.

Future metrology development of surface wrinkling will likely take advantage of the technique's sensitivity to the particular stress state within the film, which can control not only the amplitude of the instability patterns but also its orientation. Surface wrinkling has the ability to probe the residual stress state in thin films,^[61] and the onset and growth of wrinkling patterns can be used to examine properties, such as the coefficient of thermal expansion or dimensional changes caused by other external stimuli such as light or chemical vapors. Systems undergoing surface wrinkling can thus be employed as sensing platforms that react topographically to an applied or induced force within the film-substrate system. In certain cases, such as with the diffusion of solvent vapor into a film, the growth of wrinkling patterns can go beyond simply sensing the presence of a chemical and offer additional powerful insights about the diffusion kinetics within the film.^[15] Another topic for future consideration will be the use of dynamic surface wrinkling,

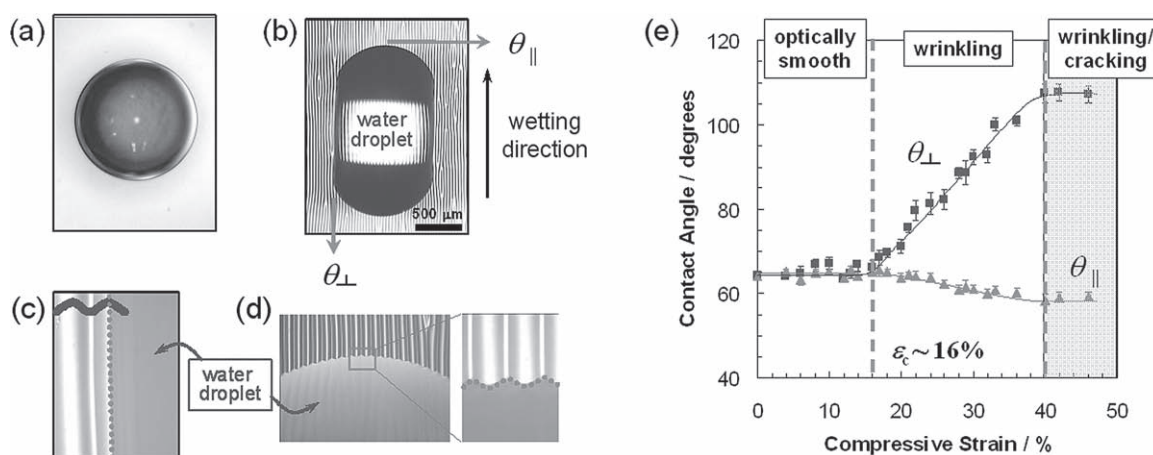


Figure 22. a) Top view, optical microscopy image of $\approx 2 \mu\text{L}$ water droplet on the smooth surface. Optical microscopy images of b) a water droplet on the patterned surface ($\epsilon = 30\%$), revealing an elongated, parallel-sided shape, c) droplet showing evidence of pinning of contact line perpendicular to the grooves, and d) droplet spreading along the grooves. The arrows in (b) indicate the direction of contact-angle measurements. e) Dependence of the water CAs in two directions (θ_{\perp} and θ_{\parallel}) on sinusoidally patterned surfaces as a function of degree of compression (ϵ). The lines are meant to guide the eye and the error bars represent one standard deviation of the data, which is taken as the experimental uncertainty of the measurement. Reproduced with permission.^[19] Copyright 2007, RSC.

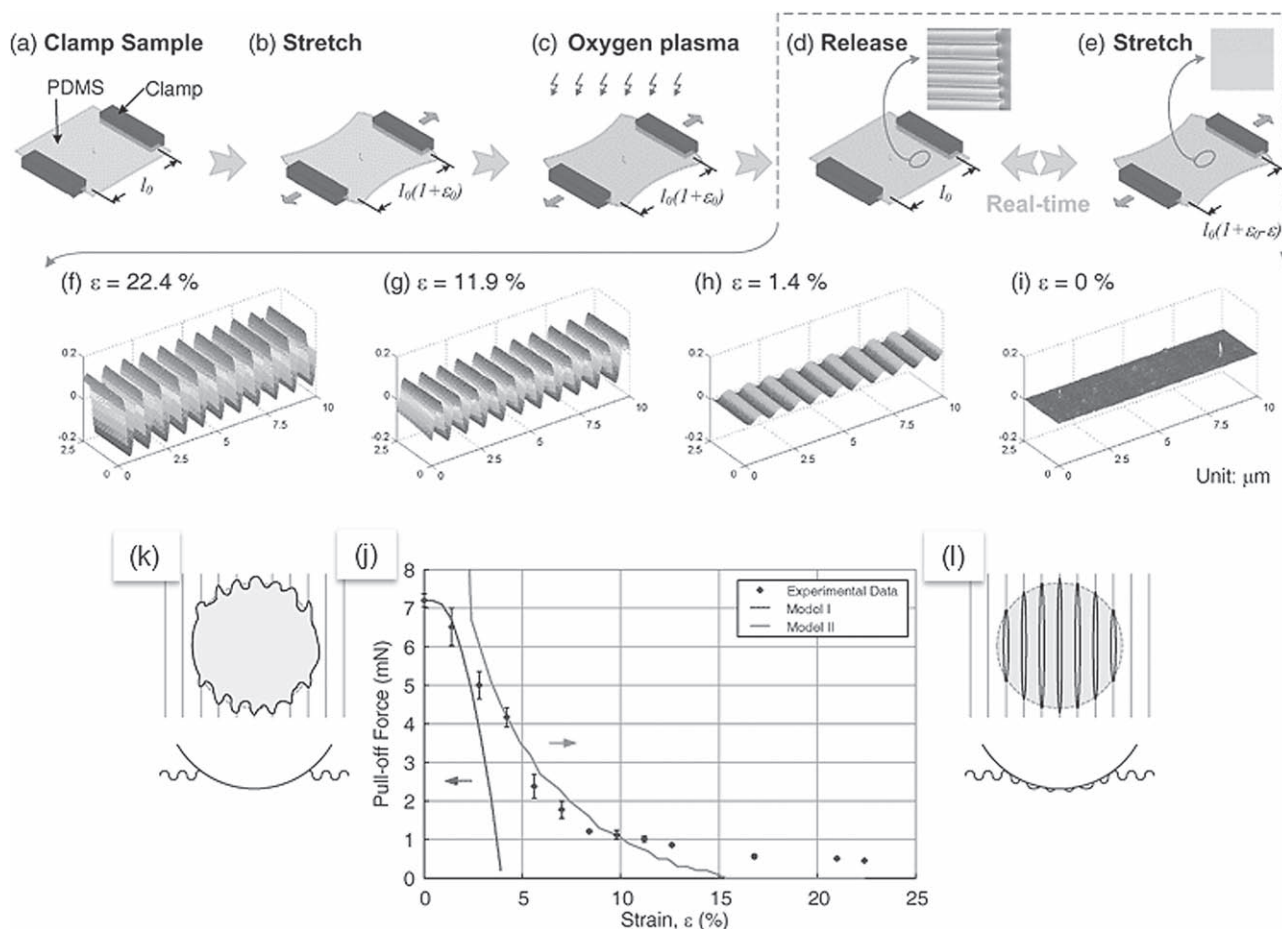


Figure 23. a–e) Schematic illustration of the fabrication of rippled PDMS film. Steps are: a) clamp PDMS film, b) stretch PDMS film to a designated strain value, c) oxygen plasma treatment, d) release stretch of the PDMS/oxide bilayer and spontaneous formation of ripple patterns, e) stretch back to the initial strain value and the ripple patterns disappear. f–i) 3D surface contour of rippled surfaces measured by AFM and plotted using Matlab. j) Comparison of experimental pull-off force versus strain to theoretical predictions from two limiting cases of contact mechanics models. k) Model I for low roughness and deep indentation; ripples flatten everywhere in the contact area except very near the contact edge. l) Model II for high roughness and shallow indentation; ripples are partially flattened. Reproduced with permission.^[121] Copyright 2008, RSC.

where the instability patterns in a film–substrate system are examined under variable frequency cyclic loading; this may provide an opportunity for studying the dynamic mechanical properties of thin film systems.

In addition to expanding the ease and speed with which measurements can be performed on thin-film materials, surface wrinkling has shown considerable promise as a method for patterning and organizing materials on the micro to nanoscale. Fery and coworkers have demonstrated, for example, the ability to do lithography-free directed colloidal assembly, with the topological features of an instability directing colloidal crystallization within the valleys of the surface wrinkles.^[127] Rogers and coworkers have shown that wrinkling provides a facile method of controllably distributing strain within a material for stretchy electronics applications, whereby thin films of conductors can be compressed and stretched without fracture due to the regular, accordion-like packing of the surface film that occurs upon onset of the instability.^[12] In some cases, changes in electronic properties that accompany material compression and wrinkling can be measured directly, as has been demonstrated

recently for strips of silicon and carbon nanotubes.^[12,40] These and similar research efforts have direct applicability to next-generation applications such as wearable computers, flexible displays, and solar panels, where nanoscale structures of conventional electronic materials will be integrated with polymers and organic compounds. Surface wrinkling methods are uniquely positioned to address the challenges involved in creating and characterizing such hybrid systems.^[48]

Given the rapid growth in the use and study of various mechanical instability methods, as well as their demonstrated applicability for a wide variety of materials systems, it is reasonable to assume that such techniques will continue to play an important role in the development and characterization of new technologies. By focusing on surface instabilities in the current Review, we have attempted to show, using brief snapshots of various aspects of the field, the remarkable breadth of applications and creative methods that have been developed by various research groups within a relatively short time period. It is our expectation that surface wrinkling and related techniques will continue to grow in popularity as they find new applications

and uses in materials science, where ever-shrinking length scales and new materials development continue to challenge existing patterning and characterization technologies.

Acknowledgements

A.J.N. acknowledges the NIST/National Research Council Postdoctoral Fellowship Program for funding. This article, a contribution of the National Institute of Standards and Technology, is not subject to US copyright. Certain equipment and instruments or materials are identified in the paper to adequately specify the experimental details. Such identification does not imply recommendation or endorsement by the National Institute of Standards and Technology, nor does it imply the materials are necessarily the best available for the purpose. This article is part of a Special Issue on Materials Science at the National Institute of Standards and Technology (NIST).

Received: May 12, 2010

Published online: September 2, 2010

-
- [1] M. Lazzari, M. A. Lopez-Quintela, *Adv. Mater.* **2003**, *15*, 1583.
 [2] L. Q. Wu, G. F. Payne, *Trends Biotechnol.* **2004**, *22*, 593.
 [3] J. V. Barth, G. Costantini, K. Kern, *Nature* **2005**, *437*, 671.
 [4] N. Bowden, S. Brittain, A. G. Evans, J. W. Hutchinson, G. M. Whitesides, *Nature* **1998**, *393*, 146.
 [5] N. Bowden, W. T. S. Huck, K. E. Paul, G. M. Whitesides, *Appl. Phys. Lett.* **1999**, *75*, 2557.
 [6] W. T. S. Huck, N. Bowden, P. Onck, T. Pardoën, J. W. Hutchinson, G. M. Whitesides, *Langmuir* **2000**, *16*, 3497.
 [7] D. B. H. Chua, H. T. Ng, S. F. Y. Li, *Appl. Phys. Lett.* **2000**, *76*, 721.
 [8] E. Cerda, L. Mahadevan, *Phys. Rev. Lett.* **2003**, *90*, 074302.
 [9] P. J. Yoo, K. Y. Suh, H. Kang, H. H. Lee, *Phys. Rev. Lett.* **2004**, *93*, 034301.
 [10] C. M. Stafford, C. Harrison, K. L. Beers, A. Karim, E. J. Amis, M. R. Vanlandingham, H. C. Kim, W. Volksen, R. D. Miller, E. E. Simonyi, *Nat. Mater.* **2004**, *3*, 545.
 [11] K. Efimenko, M. Rackaitis, E. Manias, A. Vaziri, L. Mahadevan, J. Genzer, *Nat. Mater.* **2005**, *4*, 293.
 [12] D. Y. Khang, H. Q. Jiang, Y. Huang, J. A. Rogers, *Science* **2006**, *311*, 208.
 [13] J. Genzer, J. Groenewold, *Soft Matter* **2006**, *2*, 310.
 [14] E. P. Chan, A. J. Crosby, *Soft Matter* **2006**, *2*, 324.
 [15] J. Y. Chung, A. J. Nolte, C. M. Stafford, *Adv. Mater.* **2009**, *21*, 1358.
 [16] J. Yin, Z. X. Cao, C. R. Li, I. Sheinman, X. Chen, *Proc. Natl. Acad. Sci. USA* **2008**, *105*, 19132.
 [17] H. X. Mei, R. Huang, J. Y. Chung, C. M. Stafford, H. H. Yu, *Appl. Phys. Lett.* **2007**, *90*, 151902.
 [18] M. Guvendiren, S. Yang, J. A. Burdick, *Adv. Funct. Mater.* **2009**, *19*, 3038.
 [19] H. G. Allen, *Analysis and Design of Structural Sandwich Panels*, Pergamon Press, New York **1969**.
 [20] A. Ghatak, M. K. Chaudhury, V. Shenoy, A. Sharma, *Phys. Rev. Lett.* **2000**, *85*, 4329.
 [21] E. Cerda, K. Ravi-Chandar, L. Mahadevan, *Nature* **2002**, *419*, 579.
 [22] G. Reiter, M. Hamieh, P. Damman, S. Sclavons, S. Gabriele, T. Vilmin, E. Raphael, *Nat. Mater.* **2005**, *4*, 754.
 [23] J. Y. Chung, K. H. Kim, M. K. Chaudhury, J. Sarkar, A. Sharma, *Eur. Phys. J. E: Soft Matter Biol. Phys.* **2006**, *20*, 47.
 [24] J. Huang, M. Juskiewicz, W. H. de Jeu, E. Cerda, T. Emrick, N. Menon, T. P. Russell, *Science* **2007**, *317*, 650.
 [25] E. Hamm, P. Reis, M. LeBlanc, B. Roman, E. Cerda, *Nat. Mater.* **2008**, *7*, 386.
 [26] L. Pociavsek, B. Leahy, N. Holten-Andersen, B. H. Lin, K. Y. C. Lee, E. Cerda, *Soft Matter* **2009**, *5*, 1963.
 [27] A. Strojny, X. Y. Xia, A. Tsou, W. W. Gerberich, *J. Adhes. Sci. Technol.* **1998**, *12*, 1299.
 [28] M. R. Vanlandingham, J. S. Villarrubia, W. F. Guthrie, G. F. Meyers, *Macromol. Symp.* **2001**, *167*, 15.
 [29] J. M. Kranenburg, C. A. Tweedie, K. J. van Vliet, U. S. Schubert, *Adv. Mater.* **2009**, *21*, 3551.
 [30] C. M. Stafford, B. D. Vogt, C. Harrison, D. Julthongpiput, R. Huang, *Macromolecules* **2006**, *39*, 5095.
 [31] C. M. Stafford, S. Guo, C. Harrison, M. Y. M. Chiang, *Rev. Sci. Instr.* **2005**, *76*, 062207.
 [32] C. Jiang, S. Singamaneni, E. Merrick, V. V. Tsukruk, *Nano Lett.* **2006**, *6*, 2254.
 [33] J. M. Torres, C. M. Stafford, B. D. Vogt, *ACS Nano* **2009**, *3*, 2677.
 [34] A. J. Nolte, M. F. Rubner, R. E. Cohen, *Macromolecules* **2005**, *38*, 5367.
 [35] C. H. Lu, I. Donch, M. Nolte, A. Fery, *Chem. Mater.* **2006**, *18*, 6204.
 [36] E. A. Wilder, S. Guo, S. Lin-Gibson, M. J. Fasolka, C. M. Stafford, *Macromolecules* **2006**, *39*, 4138.
 [37] H.-J. Choi, J.-H. Kim, H.-J. Lee, S.-A. Song, H.-J. Lee, J.-H. Han, M.-W. Moon, *Exp. Mech.* **2010**, *50*, 635.
 [38] H. Huang, J. Y. Chung, A. J. Nolte, C. M. Stafford, *Chem. Mater.* **2007**, *19*, 6555.
 [39] M. Wang, J. E. Comrie, Y. P. Bai, X. M. He, S. Y. Guo, W. T. S. Huck, *Adv. Funct. Mater.* **2009**, *19*, 2236.
 [40] D. Y. Khang, J. L. Xiao, C. Kocabas, S. MacLaren, T. Banks, H. Q. Jiang, Y. Y. G. Huang, J. A. Rogers, *Nano Lett.* **2008**, *8*, 124.
 [41] T. Choi, J. H. Jang, C. K. Ullal, M. C. LeMieux, V. V. Tsukruk, E. L. Thomas, *Adv. Funct. Mater.* **2006**, *16*, 1324.
 [42] H. Watanabe, T. Ohzono, T. Kunitake, *Macromolecules* **2007**, *40*, 1369.
 [43] H. Watanabe, E. Muto, T. Ohzono, A. Nakao, T. Kunitake, *J. Mater. Chem.* **2009**, *19*, 2425.
 [44] R. Vendamme, T. Ohzono, A. Nakao, M. Shimomura, T. Kunitake, *Langmuir* **2007**, *23*, 2792.
 [45] J. Y. Lee, K. E. Su, E. P. Chan, Q. L. Zhang, T. Errnick, A. J. Crosby, *Macromolecules* **2007**, *40*, 7755.
 [46] C. Dutriez, K. Satoh, M. Kamigaito, H. Yokoyama, *Macromolecules* **2007**, *40*, 7433.
 [47] D. Takh, H. H. Lee, D. Y. Khang, *Macromolecules* **2009**, *42*, 7079.
 [48] D. Y. Khang, J. A. Rogers, H. H. Lee, *Adv. Funct. Mater.* **2009**, *19*, 1526.
 [49] A. Schweikart, A. Fery, *Microchim. Acta* **2009**, *165*, 249.
 [50] L. D. Landau, E. M. Lifshitz, *Theory of Elasticity*, Pergamon Press, New York **1986**.
 [51] G. S. Gough, C. F. Elam, N. D. De Bruyne, *J. R. Aeronaut. Soc.* **1940**, *44*, 12.
 [52] A. L. Volynskii, S. Bazhenov, O. V. Lebedeva, N. F. Bakeev, *J. Mater. Sci.* **2000**, *35*, 547.
 [53] R. Huang, *J. Mech. Phys. Solids* **2005**, *53*, 63.
 [54] R. Huang, Z. Suo, *J. Appl. Phys.* **2002**, *91*, 1135.
 [55] J. Groenewold, *Physica A* **2001**, *298*, 32.
 [56] M. A. Biot, *J. Appl. Mech.* **1937**, *4*, 1.
 [57] H. Q. Jiang, D. Y. Khang, J. Z. Song, Y. G. Sun, Y. G. Huang, J. A. Rogers, *Proc. Natl. Acad. Sci. USA* **2007**, *104*, 15607.
 [58] J. Song, H. Jiang, Y. Huang, J. A. Rogers, *J. Vac. Sci. Technol., A* **2009**, *27*, 1107.
 [59] C. Harrison, C. M. Stafford, W. H. Zhang, A. Karim, *Appl. Phys. Lett.* **2004**, *85*, 4016.
 [60] C. M. Stafford, C. Harrison, in *Encyclopedia of Materials: Science and Technology (Online Updates)*, (Eds: K. H. Jürgen Buschow, R. W. Cahn, M. C. Flemings, B. Ilshner, E. J. Kramer, S. Mahajan, P. Veyssi ere), Elsevier, **2006**, 1.

- [61] J. Y. Chung, T. Q. Chastek, M. J. Fasolka, H. W. Ro, C. M. Stafford, *ACS Nano* **2009**, *3*, 844.
- [62] E. P. Chan, K. A. Page, S. H. Im, D. L. Patton, R. Huang, C. M. Stafford, *Soft Matter* **2009**, *5*, 4638.
- [63] C. M. Stafford, K. E. Roskov, T. H. Epps, M. J. Fasolka, *Rev. Sci. Instr.* **2006**, *77*, 023908.
- [64] J. C. Meredith, A. Karim, E. J. Amis, *MRS Bull.* **2002**, *27*, 330.
- [65] M. J. Fasolka, C. M. Stafford, K. L. Beers, *Adv. Polym. Sci.* **2010**, *225*, 63.
- [66] K. K. Phani, S. K. Niyogi, *J. Mater. Sci.* **1987**, *22*, 257.
- [67] A. J. Nolte, R. E. Cohen, M. F. Rubner, *Macromolecules* **2006**, *39*, 4841.
- [68] Z. Gemici, P. Smadbeck, M. F. Rubner, R. E. Cohen, *Abstr. Pap. Am. Chem. Soc.* **2008**, *235*, 186.
- [69] R. Gunawidjaja, C. Y. Jiang, H. H. Ko, V. V. Tsukruk, *Adv. Mater.* **2006**, *18*, 2895.
- [70] R. Gunawidjaja, C. Y. Jiang, S. Peleshanko, M. Ornatska, S. Singamaneni, V. V. Tsukruk, *Adv. Funct. Mater.* **2006**, *16*, 2024.
- [71] C. Y. Jiang, V. V. Tsukruk, *Adv. Mater.* **2006**, *18*, 829.
- [72] C. Y. Jiang, X. Y. Wang, R. Gunawidjaja, Y. H. Lin, M. K. Gupta, D. L. Kaplan, R. R. Naik, V. V. Tsukruk, *Adv. Funct. Mater.* **2007**, *17*, 2229.
- [73] Y. H. Lin, C. Jiang, J. Xu, Z. Q. Lin, V. V. Tsukruk, *Soft Matter* **2007**, *3*, 432.
- [74] D. Zimnitsky, C. Y. Jiang, J. Xu, Z. Q. Lin, V. V. Tsukruk, *Langmuir* **2007**, *23*, 4509.
- [75] D. Zimnitsky, C. Y. Jiang, J. Xu, Z. Q. Lin, L. Zhang, V. V. Tsukruk, *Langmuir* **2007**, *23*, 10176.
- [76] D. Zimnitsky, V. V. Shevchenko, V. V. Tsukruk, *Langmuir* **2008**, *24*, 5996.
- [77] A. J. Nolte, N. D. Treat, R. E. Cohen, M. F. Rubner, *Macromolecules* **2008**, *41*, 5793.
- [78] A. V. Tobolsky, M. C. Shen, *J. Phys. Chem.* **1963**, *67*, 1886.
- [79] A. S. Hoffman, *Adv. Drug Delivery Rev.* **2002**, *54*, 3.
- [80] N. A. Peppas, J. Z. Hilt, A. Khademhosseini, R. Langer, *Adv. Mater.* **2006**, *18*, 1345.
- [81] K. A. Aamer, C. M. Stafford, L. J. Richter, J. Kohn, M. L. Becker, *Macromolecules* **2009**, *42*, 1212.
- [82] J. Xiao, H. Jiang, D. Y. Khang, J. Wu, Y. Huang, J. A. Rogers, *J. Appl. Phys.* **2008**, *104*, 033543.
- [83] M. Alcoutlabi, G. B. McKenna, *J. Phys.: Condens. Matter* **2005**, *17*, R461.
- [84] S. Kim, C. B. Roth, J. M. Torkelson, *J. Polym. Sci., Part B: Polym. Phys.* **2008**, *46*, 2754.
- [85] R. Huang, C. M. Stafford, B. D. Vogt, *J. Aero. Eng.* **2007**, *20*, 38.
- [86] K. Van Workum, J. J. de Pablo, *Nano Lett.* **2003**, *3*, 1405.
- [87] T. R. Böhme, J. J. de Pablo, *J. Chem. Phys.* **2002**, *116*, 9939.
- [88] X. Chen, J. W. Hutchinson, *Scr. Mater.* **2004**, *50*, 797.
- [89] T. Ohzono, M. Shimomura, *Phys. Rev. B* **2004**, *69*, 132202.
- [90] M. W. Moon, S. H. Lee, J. Y. Sun, K. H. Oh, A. Vaziri, J. W. Hutchinson, *Proc. Natl. Acad. Sci. USA* **2007**, *104*, 1130.
- [91] G. X. Cao, X. Chen, C. R. Li, A. Ji, Z. X. Cao, *Phys. Rev. Lett.* **2008**, *100*, 036102.
- [92] A. Chiche, C. M. Stafford, J. T. Cabral, *Soft Matter* **2008**, *4*, 2360.
- [93] T. Ohzono, H. Watanabe, R. Vendamme, C. Kamaga, T. Kunitake, T. Ishihara, M. Shimomura, *Adv. Mater.* **2007**, *19*, 3229.
- [94] J. Yin, E. Bar-Kochba, X. Chen, *Soft Matter* **2009**, *5*, 3469.
- [95] A. K. Harris, P. Wild, D. Stopak, *Science* **1980**, *208*, 177.
- [96] K. Burton, D. L. Taylor, *Nature* **1997**, *385*, 450.
- [97] K. Burton, J. H. Park, D. L. Taylor, *Mol. Biol. Cell* **1999**, *10*, 3745.
- [98] G. Bao, S. Suresh, *Nat. Mater.* **2003**, *2*, 715.
- [99] X. Y. Jiang, S. Takayama, X. P. Qian, E. Ostuni, H. K. Wu, N. Bowden, P. LeDuc, D. E. Ingber, G. M. Whitesides, *Langmuir* **2002**, *18*, 3273.
- [100] M. T. Lam, W. C. Clem, S. Takayama, *Biomaterials* **2008**, *29*, 1705.
- [101] H. Vandeparre, P. Damman, *Phys. Rev. Lett.* **2008**, *101*, 124301.
- [102] B. A. Grzybowski, K. J. M. Bishop, C. J. Campbell, M. Fialkowski, S. K. Smoukov, *Soft Matter* **2005**, *1*, 114.
- [103] N. L. Thomas, A. H. Windle, *Polymer* **1982**, *23*, 529.
- [104] P. J. McDonald, J. Godward, R. Sackin, R. P. Sear, *Macromolecules* **2001**, *34*, 1048.
- [105] J. Kim, H. H. Lee, *J. Polym. Sci., Part B: Polym. Phys.* **2001**, *39*, 1122.
- [106] P. J. Yoo, H. H. Lee, *Phys. Rev. Lett.* **2003**, *91*, 154502.
- [107] P. J. Yoo, H. H. Lee, *Macromolecules* **2005**, *38*, 2820.
- [108] C. W. Frank, V. Rao, M. M. Despotopoulou, R. F. W. Pease, W. D. Hinsberg, R. D. Miller, J. F. Rabolt, *Science* **1996**, *273*, 912.
- [109] L. F. Francis, A. V. McCormick, D. M. Vaessen, J. A. Payne, *J. Mater. Sci.* **2002**, *37*, 4897.
- [110] Y. J. Tang, J. Chen, Y. B. Huang, D. C. Li, S. S. Wang, Z. H. Li, W. D. Zhang, *J. Micromech. Microeng.* **2007**, *17*, 1923.
- [111] W. Barthlott, C. Neinhuis, *Planta* **1997**, *202*, 1.
- [112] T. L. Sun, L. Feng, X. F. Gao, L. Jiang, *Acc. Chem. Res.* **2005**, *38*, 644.
- [113] K. Autumn, Y. A. Liang, S. T. Hsieh, W. Zesch, W. P. Chan, T. W. Kenny, R. Fearing, R. J. Full, *Nature* **2000**, *405*, 681.
- [114] M. Scherge, S. Gorb, *Biological micro- and nanotribology: Nature's solutions*, Springer Verlag, Berlin **2001**.
- [115] J. Y. Chung, M. K. Chaudhury, *J. R. Soc., Interface* **2005**, *2*, 55.
- [116] A. Majumder, A. Ghatak, A. Sharma, *Science* **2007**, *318*, 258.
- [117] F. Xia, L. Jiang, *Adv. Mater.* **2008**, *20*, 2842.
- [118] D. C. Hyun, G. D. Moon, E. C. Cho, U. Y. Jeong, *Adv. Funct. Mater.* **2009**, *19*, 2155.
- [119] J. Y. Chung, J. P. Youngblood, C. M. Stafford, *Soft Matter* **2007**, *3*, 1163.
- [120] P. C. Lin, S. Yang, *Soft Matter* **2009**, *5*, 1011.
- [121] P. C. Lin, S. Vajpayee, A. Jagota, C. Y. Hui, S. Yang, *Soft Matter* **2008**, *4*, 1830.
- [122] K. Khare, J. Zhou, S. Yang, *Langmuir* **2009**, *25*, 12794.
- [123] E. P. Chan, E. J. Smith, R. C. Hayward, A. J. Crosby, *Adv. Mater.* **2008**, *20*, 711.
- [124] C. J. Rand, A. J. Crosby, *J. Appl. Phys.* **2009**, *106*, 064913.
- [125] T. Ohzono, H. Monobe, K. Shiokawa, M. Fujiwara, Y. Shimizu, *Soft Matter* **2009**, *5*, 4658.
- [126] K. Efirnenko, J. Finlay, M. E. Callow, J. A. Callow, J. Genzer, *ACS Appl. Mater. Interfaces* **2009**, *1*, 1031.
- [127] C. H. Lu, H. Mohwald, A. Fery, *Soft Matter* **2007**, *3*, 1530.